Circulation patterns and implication for fine sediment transport in a preserved tropical estuary: The case of the Maroni (French Guiana)

Anh T.K. Do, Aldo Sottolichio, Nicolas Huybrechts, Antoine Gardel

Circulation patterns and implication for fine sediment transport in a preserved tropical estuary: The case of the Maroni (French Guiana)

Anh T.K. Do [a,b,*], Aldo Sottolichio [c], Nicolas Huybrechts [a], Antoine Gardel [d]

[a] Cerema, HA Research Team, 134 rue de Beauvais – CS 60039-60280 Margny-lès-Compiègne, France [b] The University of Da Nang (UD)–University of Science and Technology (DUT), Da Nang, Viet Nam
[c] University of Bordeaux, UMR 5805 CNRS - EPOC, 33615 Pessac, France
[d] CNRS, USR 3456 LEEISA, Centre de recherche de Montabo, IRD, 97300 Cayenne, France

Abstract

Compared to temperate estuaries, tropical ones are less documented. Among them, the numerous estuaries along the Guiana shoreline present at least two original features: they are still preserved from anthropogenic modifications, and their hydro-morphodynamics are influenced by longshore migration of outer coastal mud banks. This study deals with the Maroni estuary, a mesotidal preserved tropical estuary, currently spotting more attention to better anticipate changes related to the development of harbour activities. Field data collected over semi-diurnal tidal cycles in the lower estuary revealed the presence of a turbidity maximum and seasonally contrasted hydro-sedimentary features. A one-year 3D hydrodynamic simulation covering a wide-range of tidal and fluvial conditions was performed to further analyse the seasonal variability of stratification and residual circulation patterns. The estuary is well-mixed for a very low river discharge (lower than 200 m^3/s). It becomes partly mixed in both spring and neap tide in case of a moderate river discharge of 700 m^3/s. The strongest stratification, which could be associated to a salt wedge near the mouth, appears during neap tides combined with higher discharge. Residual currents along the navigation channel are usually seaward except during neap tides when the discharge is large enough (700 m^3/s) to generate stratification and landward residual current near the bottom to mid depth until the first km 15 from the mouth. Residual inflow starts from the location of the mud bank and extends along the navigation channel near the eastern bank. The inflow extension matches with observed highly turbid areas and fresh mud deposits, suggesting an outer supply of mud. In summary, this exploratory work allows a first description of current dynamics of the Maroni, and is a first step before a comprehensive study of changes in estuarine circulation and fine sediment transport under different configurations of coastal mud banks.

Keywords : Tropical estuary-Estuarine sediment dynamic-Mud bank-Residual current-Stratification-Turbidity maximum

1. Introduction

Located between 30°N and 30°S of latitude, tropical estuaries are frequently fringed by dense mangroves (Anthony, 2004, Bomer et al., 2020, Van Santen et al., 2007, Victor et al., 2004, Willemsen et al., 2016) or muddy coastal environment (Anthony, 2006, Chapman, 1974, Lugo and Snedaker, 1974, Wong and Tam, 2012). In contrast compared to temperate estuaries, the functioning of hydro-sedimentary dynamics in tropical estuaries is less understood and studies are still sparse (Kitheka, 1997, Anthony and Dolique, 2004, Capo et al., 2006, Asp et al., 2018) as for instance for estuaries along the Guiana coastline in South America. The originality of these latter stands in the presence of fine sediment mostly originated from offshore supply whereas rivers rather bring coarse sandy material (Jouanneau and Pujos, 1987, Jounneau and Pujos, 1988). It is the opposite configuration compared to many temperate estuaries where the muddy content comes from riverine contribution and the sandy material is located near the mouth as a result of inflow from the coastal area (Fettweis et al., 1998, Uncles et al., 1985).

The Maroni is one of the largest estuaries along the Guiana coast in terms of width and river flow rate. However, few studies on its dynamics have been conducted, and they are mainly based on short-term data acquisition or geochemical evidence (Berthois and Hoorelbeck, 1968, Jounneau and Pujos, 1988). Only recently, the Maroni and other neighbouring estuaries have spotted back the attention, as a significant demographic growth is expected, more especially along rivers and shoreline in French Guiana. One of the new observations of hydrodynamics was conducted by Ross et al. (2019), which

focused on a high river flow event to investigate subtidal circulation patterns. In terms of human impacts, the last dredging operation on the Maroni estuary occurred 25 years ago and to date no bridge or huge coastal structure have been built yet. It thus presents a rare chance to analyse circulation patterns and forcing mechanisms in a natural estuary (Ross et al., 2019).

For these different reasons, a deeper and updated description of the Maroni dynamics is thus needed in order to better anticipate changes related to the development of harbour activities and to the arrival of a coastal mud bank near the navigation channel (Jolivet et al., 2019). With such a perspective in mind, different field surveys are conducted on the downstream part of the Maroni estuary during low and high river discharges. Since field data are still limited in space and duration due to difficult logistic conditions for field monitoring, a 3D hydrodynamic numerical model is also built to further explore different flow conditions. Different numerical models have already been developed to analyse the current and salinity on the Guiana continental shelf (Chevalier et al., 2004, Bourret et al., 2008) or the turbid plume around mud banks (Chevalier et al., 2008). Based on finite difference techniques, these previous models focus on the coastal dynamics along French Guiana coast but they were not used to analyse estuarine dynamics because of the lack of validation data and the poor mesh description inside the rivers. Even if this study focus on the particular case of the Maroni, results serve to lighten the estuarine dynamic of Guiana estuaries or more generally of estuaries influenced by a sediment source from adjacent sea area (Xiao et al., 2018, Shimozono et al., 2019, Wright, 1989). To reach these aims, first, collected in situ data are described for different flow rates and tidal amplitudes. This allows us to identify the length of salinity intrusion and to highlight the variation of velocity strength and concentration level inside the downstream estuary. Then, numerical results are exploited: (1) to investigate the interactions between stratification, circulation and residual current; (2) to provide insight about driving processes of the circulation; and (3) to deduce implication for sediment transport inside the central part of the estuary.

2. Regional context

Located at the border between Suriname and French Guiana, the Maroni estuary (Fig. 1) ends up inside the Amazonian mud banks system (Anthony et al., 2010). These coastal mud banks come from the part of the Amazonian turbid plume which is northwest transported by the Guiana oceanic current (Wells and Coleman, 1981). Once the turbid suspension reaches the Guiana shelf, it is transformed into individual mud banks (Allison et al., 2000). Between the Amazon and the Orinoco (Venezuela) rivers, mud banks are generally about 15–20 spaced out 15–25 km apart. Areas between mud banks called inter-bank areas are exposed to strong waves and undergo erosion. The mud banks migrate from 1 to 5 km/yr (Gardel and Gratiot, 2005), and they can attain 5 m thick, 10 to 60 km long, and 20 to 30 km wide (Allison et al., 2000, Froidefond et al., 1988).

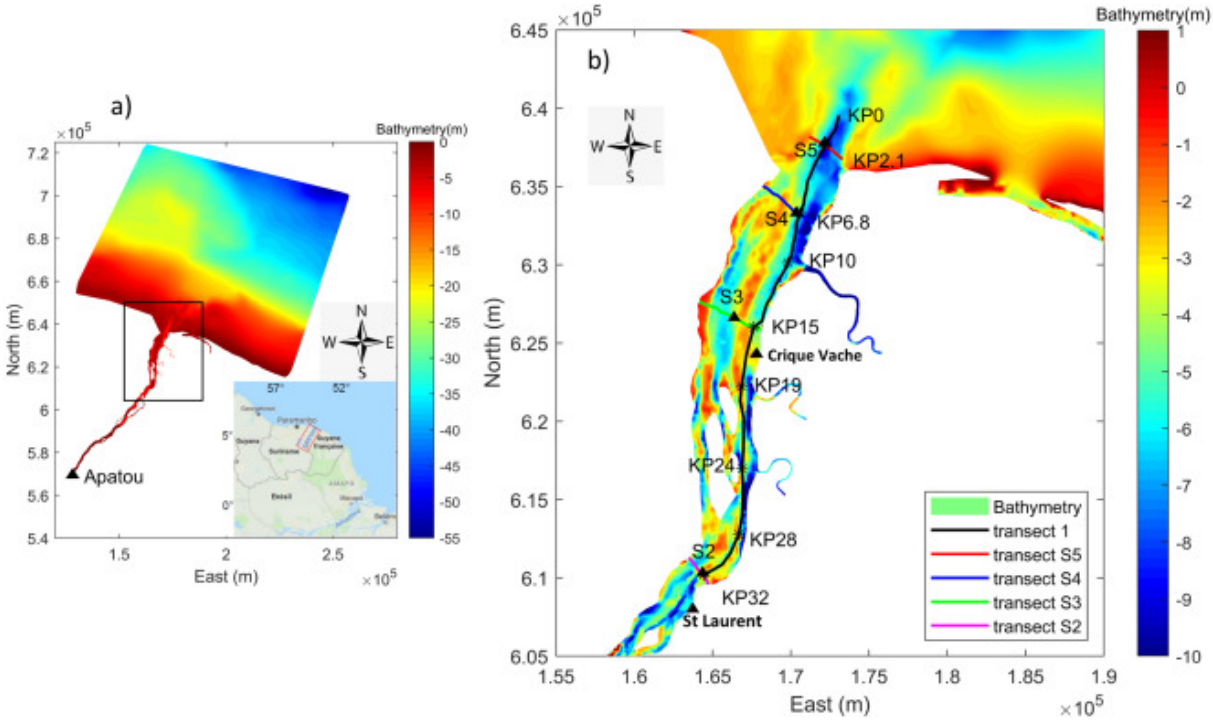

Fig. 1. The Maroni estuary. 1a bathymetry and overall location. 1b survey stations and main landmarks.

Table 1. Overview of structure of the hydrodynamic simulation considering seasonal river flow for calibration and verification.

Calibration/Validation	**Scenarios**	**Name**	**River discharge (m^3/s)**		**Station/survey date**	**Tide characteristic**
			Maroni	**Mana**		
Calibration	High river discharge (June 2017)	EH3	3850/3610	741/696	S2(14th) S3(13th) S4(13th)	Neap tides
	Low river discharge (October 2017)	EH4	582	78	S2(8th) S3(8th) S5(8th)	Spring tides
Verification	Low river discharge (November 2016)	EH1	176/182	71/65	S2 (17th) S3(15th)	Spring tides
	High river discharge (March 2017)	EH2	4770/4540	485/422	S2(15th) S3(14th)	Spring tides

During their shoreline migration along the French Guiana, Suriname and Guyana, these mud banks cross seventeen estuarine systems whose bottoms are mainly composed of sand or coarse sand in their central and upstream part. However muddy sediments are patchy observed in the downstream part. As suggested by previous studies (Jouanneau and Pujos, 1987, Jounneau and Pujos, 1988, Orseau et al., 2017), the mud bank presence at an estuary mouth constitutes a source of fine sediment that may enter these estuaries.

3. Study site

The Maroni river is 677 km long with a watershed of 60,930 km^2. In the estuarine area, its width is 700–900 m near Apatou, 100 km upstream from the mouth (KP100, Kilometric point, Fig. 1) and up to 4000–5000 m between KP7 to KP15. Small tributaries mostly on the right bank are flowing to the estuary and some islands built from alluvial deposits are present upstream Crique Vache (Fig. 1). The climate is equatorial and within the intertropical convergence zone. Well contrasted seasonal variations are characterized by a high river discharge season from late December to July, and a low river discharge season from August to December. Trade-winds are weak and characterized by a quasi-constant direction of about 10°–15° (direction from the north) throughout the year (Gratiot et al., 2007). Water discharge is estimated by Direction de l'Equipement, de l'Aménagement et du logement (DEAL) at Apatou via a rating curve. The mean annual discharge is reaching 1700 m^3/s, with lower values down to 100 m^3/s, during the low flow periods and higher values up to 5000 m^3/s during the high flow periods.

Bed material samples have been collected by Jounneau and Pujos (1988) during low (November 1984) and high (May 1985) river discharge periods. Grain-size analysis, showed that the upstream part of the estuary (upstream of St Laurent) is composed of coarse sand (mean diameter 1–2 mm) whereas fine materials are found near the mouth.

The tide propagates up to 100 km upstream from the mouth, until a natural weir at Apatou. No continuous tidal gauge is installed inside the Maroni estuary even though water levels are recorded at three locations by the Port Authorities during two months each year.

Based on a T_Tide analysis (Pawlowicz et al., 2002), Sottolichio et al. (2018) pointed out a small amplification from the mouth to Crique Vache (4 cm) and then a decrease of the tidal amplitude down to 10 cm until Saint Laurent du Maroni (KP35, SLM). The amplification is probably induced by the section reduction whereas the decrease can be due to the presence of island and a modification of the bed texture (Sottolichio et al., 2018).

Besides bed samples collection, Jounneau and Pujos (1988) also identified the position of the salinity intrusion and the turbidity maximum during low and high discharge seasons by collecting water samples and suspended matter near the surface. During low hydrological conditions, the salt intrusion (S 0.5 isohaline) reached the first islands of the estuary (approximately KP 19), while under the high river flow conditions it stayed near the mouth (around KP 5). As for the turbidity maximum, during the low hydrological condition it had suspensed sediment concentration of up to 0.9 kg/m^3 in surface water, and was located in the lower estuary (downstream of the Coswine tributary, KP 9, Fig. 1) whereas, during the high river flow event, it was less extended, less concentrated (0.3 kg/m^3) and only appeared near the mouth (KP 2 to KP 3).

Tidal variation inside the estuary is described by Berthois and Hoorelbeck (1968)through shipboard profiles at different locations. During the survey of Berthois and Hoorelbeck (1968), the measured flowrate is within 1800–2000 m^3/s, close to the mean annual discharge. The main results from their study are shortly reminded here. The mouth (KP 2, Fig. 1) already corresponds to the limit of the oceanic influence. The salinity reaches 0.2–0.5 g/kg at low tide. The bottom peak velocity has more or less the same magnitude (0.4 m/s) during the flood and ebb. Periods of low velocity near the bottom are observed both during ebb and flood. In the central part (KP 15, Fig. 1), low salinity and sediment concentrations are observed. No fine sediment is available at the bottom and the turbidity level corresponds to advection from upstream. At high tide, the slack is well pronounced and even reaches the whole water column. It however happens in a very short period. Upstream the first islands (KP 28), ebb advection dominates during 7 h. Only 2 to 4 h is available for flood. Up to now, the knowledge about sediment dynamics in Maroni estuary is based on the works of Berthois and Hoorelbeck (1968) and Jounneau and Pujos (1988). Since these two previous studies, although there is no scientific evidence, the estuary may have undergone morphodynamic evolution. It is thus necessary to update the knowledge about the circulation and the sediment transport and also to provide more details about intratidal variability (neap–spring) under a larger range of hydrological conditions. Gardel et al., this issue describe a development pattern wherein the Maroni estuary has tended to evolve towards a delta built from both Maroni river bedload and marine mud from Amazon river located approximately 750 km to the southwest.

4. Methodology

Table 2. Comparison between model results and observations in calibration.

	Parameters	RMSE			Skill	
		Station	Surface	Bottom	Surface	Bottom
EH3 Calibration	Water level (m)	SLM	0.20		0.96	
		Crique Vach				
	Velocity (m/s)	S2	0.03	0.18	0.98	0.77
		S3	0.14	0.07	0.93	0.93
		S4	0.05	0.14	0.89	0.74
	Direction ()	S2	19.73	14.47	0.96	0.95
		S3	34.72	31.39	0.89	0.91
		S4	32.55	9.55	0.89	0.96
	Salinity (g/kg)	S2	0.02	0.02	0.00	0.00
		S3	0.02	0.02	0.00	0.00
		S4	0.41	0.71	0.59	0.91

Table 3. Comparison between model results and observations in verification.

	Parameters	RMSE			Skill	
		Station	Surface	Bottom	Surface	Bottom
EH1 Verification	Water level (m)	SLM	0.06		0.98	
		Crique Vache	0.10		0.98	
	Velocity (m/s)	S2	0.08	0.16	0.76	0.53
		S3	0.16	0.08	0.83	0.82
	Direction ()	S2	31.49	25.66	0.92	0.92
		S3	57.55	16.16	0.58	0.93
	Salinity (g/kg)	S2	1.39	1.29	0.61	0.69
		S3	4.32	3.99	0.69	0.76

4.1. Field survey

Four shipboard profiling surveys (EH1 to EH4) were conducted between 2016 and 2017 during low and high river discharges with different flow conditions in terms of river discharge and tidal range (Table 1). Two stations (S2 at KP 32, S3 at KP 15 Fig. 1) are monitored during four surveys (EH1, EH2, EH3, and EH4). Another two stations located more downstream (S4 at KP 6 and S5 at KP 2) are added for surveys EH3 and EH4. During the first three surveys (EH1, EH2 and EH3), station S1 and S2 were sampled during two successive days (Table 1). During the fourth survey (EH4), the three station S2, S3 and S5 were sampled simultaneously. For each shipboard survey, data are collected every 30 min during a semi-diurnal tidal cycle (12 h 30 min): salinity using CTD (CastAway © SonTek), velocity and flow direction using a single point current meter (Aquadopp © Nortek) and turbidity using an optical (OBS 5+ © Campbell Scientific) probe. The CTD sampling frequency is 5 s^{-1}. For the Aquadopp, the sampling frequency is 1 s^{-1}. The vertical profiles are collected by moving the sensor through the water depth since

the sensor is punctual with only one cell. For the OBS 5+, the frequency is 1 s with an averaging period of 10 s. The OBS5+ measurement is based on the measurement of two optical signals: near and far field. The combination of the two signals allows to avoid saturation and thus to cover a wider range of sediment concentration than a classical OBS. Turbidity signal is converted into suspended sediment concentration (kg/m^3) using a calibration curve built in the lab with mud material collected in the field. The calibration in the lab allows to cover a range of concentration levels up to 10 kg/m^3. It should be kept in mind that the calibration is performed with only mud concentration whereas the sensor measures in the field organic and inorganic matters. An in-situ calibration would be probably more accurate but it requires a more complicated logistic to rapidly treat the water samples.

In addition, for EH3 and EH4 surveys, along-channel transects are conducted to locate salinity intrusion during low and high tide conditions using the moving vessel method (Savenije, 1989). Stratification strength is estimated using the stratification number "Sn" defined as the difference between bottom and surface salinity divided by depth averaged salinity. According to Hansen and Rattray (1966), Sn higher than 0.1 corresponds to stratified estuary whereas values higher than 1 represent estuary with salt wedge. Besides, bathymetric surveys (Fig. 1) are performed using bi-frequency sonar sensor (Midas Surveyor 210/33 kHz © Valeport) during the low river discharge survey of 2016 and 2017, in the downstream part of the estuary. The mud thickness is estimated as the vertical distance between the two signals in low and high frequency. The recorded depth is corrected from tidal elevation using three tidal stations located along the survey area.

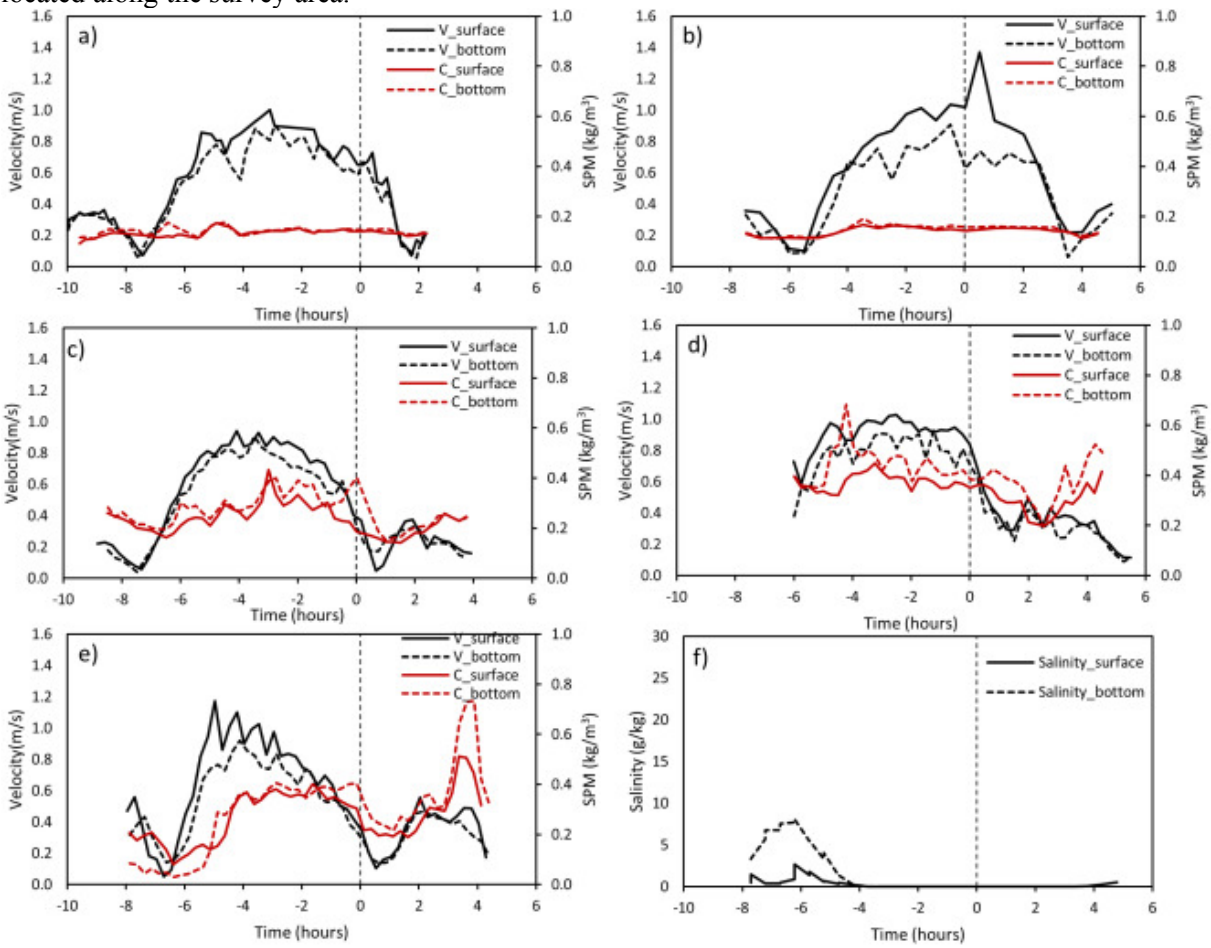

Fig. 2. Vertical variations during high river discharge. (a) S2 neap tide; (b) S2 spring tide (c) S3 neap tide, (d) S3 spring tides, (e) S4 neap tide, (f) Salinity at S4 during neap tide.

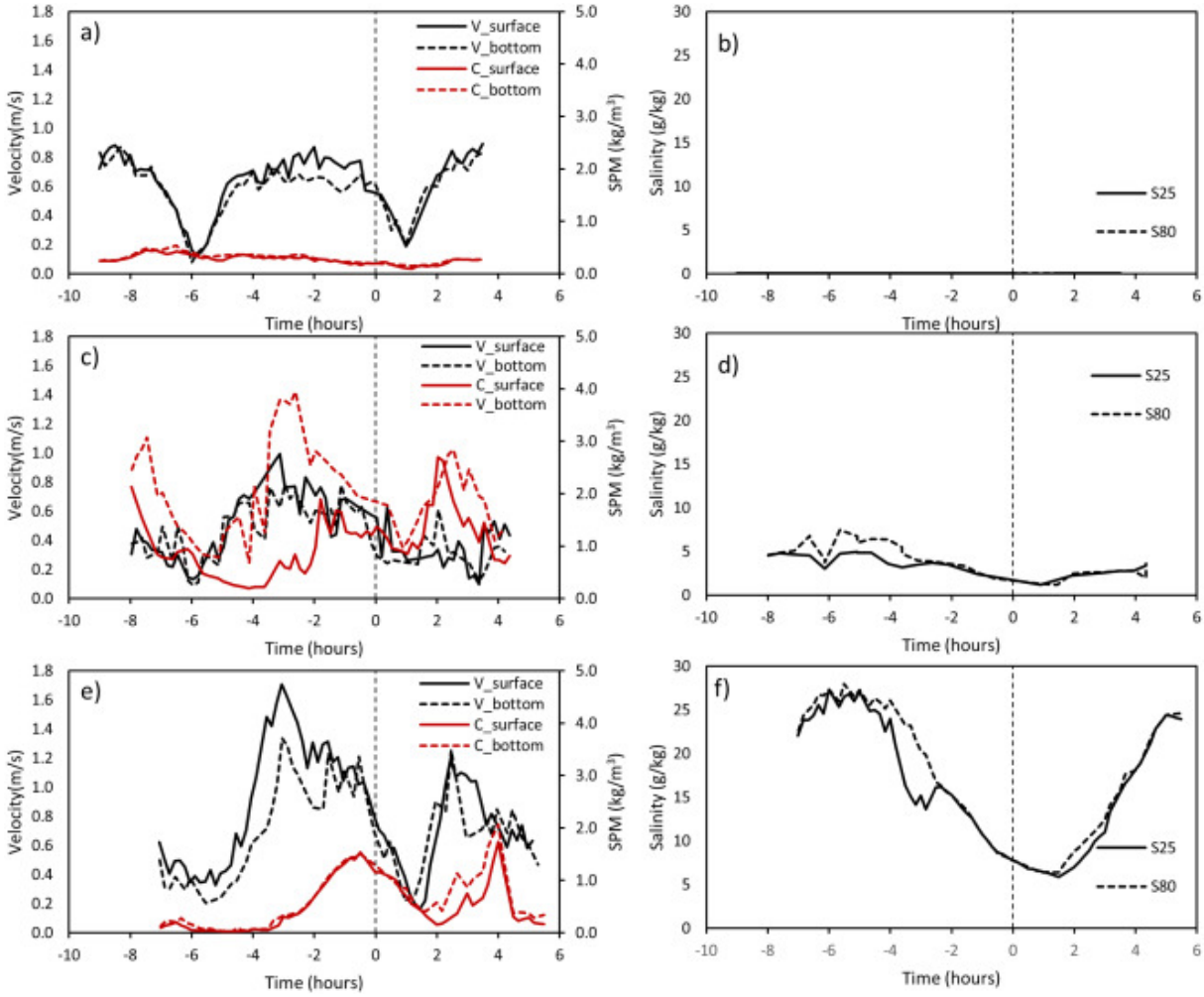

Fig. 3. Vertical variations of current velocity, salinity, and SPM at stations S2 (a&b), S3 (c&d) and S5 (e&f) during October, 2017 field campaign (low river discharge, spring tides).

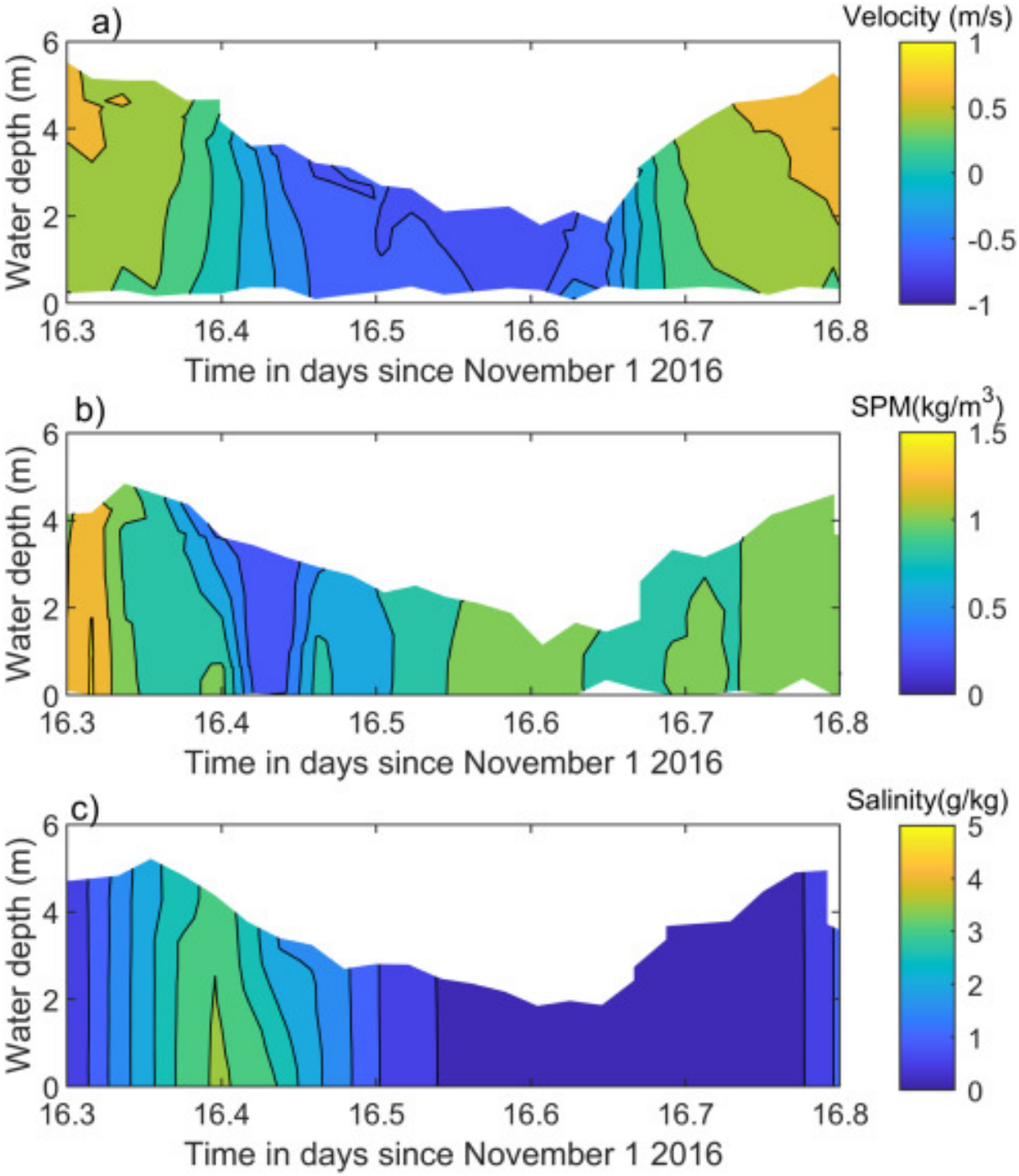

Fig. 4. Along channel velocity, SPM and salinity at S2 during pronounced low river discharge (EH1).

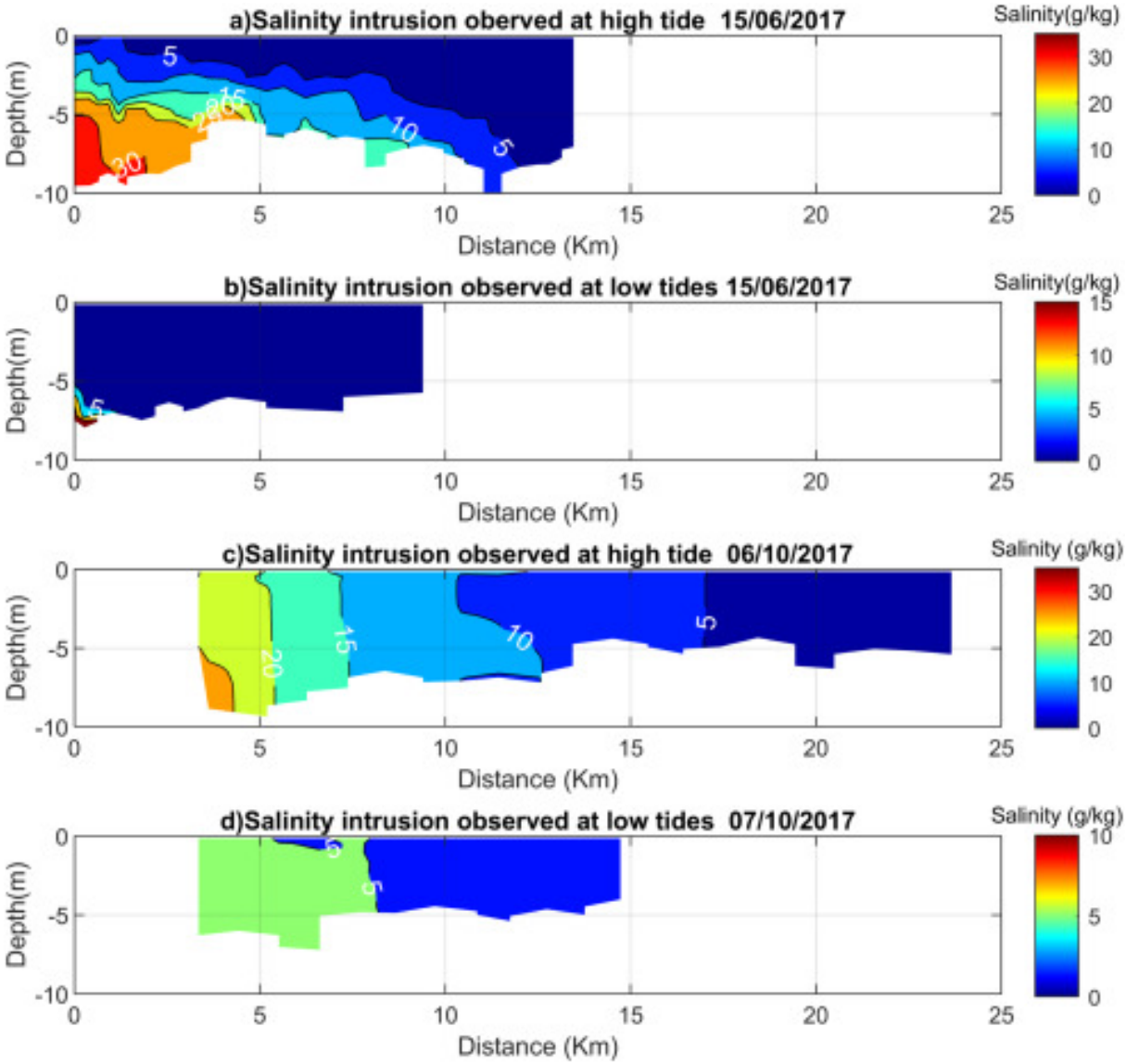

Fig. 5. Measured salinity levels measured along the navigation channel at high and low tide during wet (a, b) and dry season (c, d).

4.2. Numerical model

In this work, a 3D numerical model is built (Do et al., 2019) using the open source TELEMAC-MASCARET modelling system. TELEMAC-3D solves three-dimensional flow equations (Navier–Stokes) and transport-diffusion equations of passive tracer. The discretization in TELEMAC-3D (Hervouet, 2007) is based on finite element techniques and unstructured mesh well adapted to describe real river geometry with isles, tributaries. For the turbulence, a mixing length model is selected and combined with Lehfeldt and Bloss (1988) damping functions.

The computational domain extends into 90 km in width and 97 km in length for the coastal part. Inland, the domain extends until the limit of tide propagation, where measured river discharge is available. The distance between nodes of the horizontal mesh resolution decreases from 2.5 km in the coastal zone to 120 m inside the central part of the estuary, to 50 m in the tributaries and down to about 10 m around islands. The horizontal grid contains 19,694 nodes, 34,241 triangular elements. For the 3D mesh, 8 vertical planes are used with a finer resolution near the bottom. The distribution of vertical mesh layers from bottom to water surface have been defined as a percentage of the water depth as follows (0; 0.075; 0.15; 0.3; 0.5; 0.7; 0.85; and 1.0).

The computational domain contains three open boundaries. Upstream for Maroni and Mana rivers, daily river discharges are forced. Offshore, tidal level and currents are imposed using atlases of the Amazon

shelf from Oregon State University. The offshore imposed salinity is 35 g/kg. A time step of 20 s is used for each case investigated. Most complete surveys are selected (EH3 and EH4) for calibration (Table 1) whereas the two others (EH1 and EH2) are used for verification. TELEMAC allows to use different friction formulations and associated friction coefficients as Chezy, Manning, Strickler or Nikuradse. The friction coefficient is then converted inside the code into a no-dimensional quadratic friction coefficient. The Strickler relationship has been selected using a spatial varying friction coefficient. The Strickler's coefficient, K (m/s) is in fact the inverse value of the Manning's coefficient. Three zones of constant Manning–Strickler coefficient are defined as coastal zone (with a depth larger than 20 m), central part of the estuary (limit from St Laurent to the area with depth less than or equal 20 m) and upstream islands (upstream part of St Laurent). The Manning–Strickler friction coefficient varies from 45 (m/s) in the coastal zone, decreasing to 35 (m/s) in the estuary and to 30 (m/s) in the upstream rive part.
Model performance is quantified through root mean square error (RMSE), and predictive skill (SS) introduced by Willmott (1981). RMSE and SS are summed up in Table 2 for the calibration (EH3) and Table 3 for the verification steps (EH1). Two cases, with full data sets including water levels, velocities and salinity have been selected here.
Table 3 points out that the model results reasonably agree with the observed data for water level and velocity. The model skill score of water level (EH1) indicates the SS are almost unity (0.98) in both stations, SLM and Crique Vache. The RMSE of water levels is 0.06 m at Crique Vache and 0.1 m at SLM.
The model skill for velocity at station S2, S3 and S4 at both surface layer and bottom layer during high river discharge of calibration (EH3) indicates a very good agreement with a high skill coefficient, larger than 0.74. The average RMSE of velocity is very small (0.1 m/s) in the calibration case. In case of verification under low river discharge, EH1, the model skill for velocity at S3 also displays a very good agreement in both surface and bottom layer with a skill of 0.83 and 0.82, respectively. An exception is however observed for the skill value of bottom velocity at station S2 for the lowest discharge (EH1) with a little underestimation.

The model reproduces the seasonal variation in salinity intrusion between the low and high discharge. Salinity is observed until upstream part (KP 32) during very low discharge, EH1 while the salinity is only observed at river mouth (station S4, KP 6) for high discharge, EH3, thus skill of salinity of station S2 and S3 are nearly zero in this case (Table 2). The model skill of salinity is slightly lower than for velocities and water level except the skill coefficient of bottom velocity at station S2. However, the main hydrodynamic patterns (velocity and salinity) are well reproduced by the model for both low and high discharges.

5. Results

5.1. Observed intra-tidal and neap–spring dynamics during high river discharge

Both field surveys during high river discharges are characterized by similar value (3600 m/s) though tidal range is changing from spring to neap tide. Intra-tidal variation of measured variables is illustrated on Fig. 2 where low water slack (LWS) is selected as "zero" for the time scale to facilitate the comparison between stations and season.
During neap tides, the tidal currents outline stronger peaks in velocity during the ebb, reaching a maximum of 1 m/s at station S2 (Fig. 2a), 0.94 m/s at S3 (Fig. 2c) and 1.17 m/s at station S4 (Fig. 2e). Salinity is only noticed near the river mouth at station S4 during high tide. The salinity reaches its maximum value of 8 g/kg at the bottom during high water slack (HWS, Fig. 2f) then it rapidly decreases down to almost null value during ebb and low water slack. The vertical salinity distribution at station S4 displays a strong difference between the bottom and the surface during flood. At stations S3 and S2, salinity is lower than 0.05 g/kg for both spring and neap tides (not shown in Fig. 2).
A phase difference between current speed and water level is observed i.e., 0.54 h after low water level at station S4, 0.67 h at station S3 and 1.75 h at station S2. Durations of low water slack (LWS) increase from the river mouth (0.54 h at S4) to the upstream part since river discharge at the upper estuary gains influence. At station S2, durations of HWS and LWS are estimated as 0.56 h and 1.75 h respectively. Higher river discharge induces stronger ebb velocities and longer ebb than flood duration. SPM levels

at station S2 (Fig. 2a) are low with maximum values around 0.17 kg/m^3. A strong resuspension occurs in S4 station and creates high turbidity conditions near the bed. Main variations of SPM at S4 (Fig. 2e) is quite consistent with variation of currents. Indeed, high values of SPM correspond to high velocities and low values of SPM correspond to low velocities except during the flood very high values of SPM at the bottom (0.73 kg/m^3) are associated with low velocities.
For spring conditions during high river discharge, tidal variations are illustrated on Fig. 2b (S2) and d (S3) where SPM levels at S2 still rather correspond to fluvial advection (Fig. 2b). Higher concentration is observed near the bottom at S3 (0.68 kg/m^3) and this more particularly during the ebb (Fig. 2d). During the spring tide in a high river discharge period, the turbidity maximum is hitting S3 (KP 15) whereas previous study (Berthois and Hoorelbeck, 1968) positioned it downstream Coswine (KP 9).

5.2. Observed intra-tidal dynamics during low river discharge

Both surveys in low hydrological conditions coincide with spring tide conditions and two contrasted river discharges (600 m^3/s and 200 m^3/s). During moderate discharge (Q 600 m^3/s), current velocities at station S2 (Fig. 3a) is lower than during the high discharge events (Fig. 2a&b) and the strength of flood and ebb currents are more equivalent. However, at the middle and lower part of the estuary (station S3 and S5) current asymmetry is ebb dominant with maximum values of 1.06 m/s (Fig. 3c) and 1.7 m/s (Fig. 3e), respectively.
Concerning SPM, observed levels are increasing from the river mouth (Fig. 3e), they are reaching their maximum (3.94 kg/m^3 near the bottom, Fig. 3c) at station S3 and then they are decreasing until station S2 (Fig. 3a). At station S2 (Fig. 3a), SPM values are lower, with a maximum value of 0.54 kg/m^3 through most of the water column. The SPM variability at station S3 (Fig. 3c) is similar to S2 relying more upon velocity condition but it has a larger difference between surface and bottom layer. At the bottom layer, the SPM variation is in line with those for tidal current. It attains a minimum value at slack water and maximum value at the time of the strongest currents, suggesting a predominance of resuspension and deposition processes. Between stations S3 and S5, some differences in the SPM distribution within the water column can be noticed. At station S5 (Fig. 3e), SPM variation pattern also relies on the current conditions but there is a lag time between the current and the SPM. The lowest SPM levels occur more or less simultaneously as the lowest velocities. Nevertheless, the highest SPM does not occur in phase with the highest velocity.
Different patterns are also observed with vertical salinity distributions. At station S2 (Fig. 3b), the whole water column is nearly fresh water with a very low salinity value (0.03 g/kg). At station S3 and S5 (Fig. 3d and f), stratification is observed at HWS while salinity differences between the surface and bottom layers are smaller, indicating a stronger vertical mixing at LWS. The salinity signal at S5 points out a significant variation: salinity remained high around 28 g/kg near the bed at high tide to approximately 6 g/kg during low tide.
For the first survey in the very low hydrological condition (EH1 survey), a long low discharge period (200 m^3/s) has occurred. Observed vertical variations for current, SPM and salinity at S2 in such dry conditions are illustrated on Fig. 4. The current angle is shifted to isolate along and across the channel component. Only along channel contribution is here plotted on Fig. 4 where negative values correspond to outflow and positive ones to inflow.
As in Figs. 3a, 4a displays more balance between flood and ebb. Salinity attains a maximum value of 3.5 g/kg at the high-water slack (Fig. 4c) and a high SPM value of 1.5 kg/m^3 is noticed at the time of the strongest current (Fig. 4b). It should be also noted that during moderate flow rate, HWS are slightly longer than LWS at S2 and S3. For instance, HWS duration reaches 1.17 h and LWS 0.99 h at S2. In case of a more pronounced low river discharge, HWS duration at S2 is increasing up to 1.47 h in regards of 0.47 h for LWS.

5.3. Observed longitudinal and seasonal variability

Along-channel monitoring transects are conducted during the low (EH4) and high river discharge (EH3) under mean tidal amplitude. Both surveys lead to contrasted stratification patterns. Fig. 5 presents measured salinity levels along the navigation channel at high and low tide during high river discharge (Fig. 5a & b) and low river discharge (Fig. 5c & d). Transects with low river discharge are extended further upstream while transects at high river discharge are extended more downstream. Therefore, the starting point of transect at the high river discharge is selected as KP0 to facilitate the comparison between two seasons.

Observed flow rate at Apatou is higher than 3500 m^3/s during the high river discharge (June 2017). As isohaline 5 is clearly visible on Fig. 5a, it is selected to illustrate the seasonal and longitudinal variation. During the low river discharge (October 2017) discharge is 700 m^3/s and salt intrusion reaches KP 24 (Fig. 1). Isohaline 5 is oscillating between KP 8 and KP 17 with weak vertical gradient for both low and high tide (Fig. 5c and d). For the high river discharge, this isohaline is oscillating between KP 1 and KP 12 but stays near the bed or mid depth. A low tide, most of the estuary is characterized by a low salinity 0.5 g/kg (Fig. 5b). At high tide, salinity has propagated inside the estuary near the bottom and strong stratification is noticed with a salt wedge until KP 10.

Similarly, collected turbidity data provide additional information to the shipboard profile analysis. During low river discharge (Fig. 6a), SPM level is higher than 0.3 kg/m^3 in the whole water column except at the surface in the most upstream part. It can reach up to 4 kg/m at mid depth. The Maroni estuary appears as turbid from the mouth to KP 15–20 (S3) as already noticed in Fig. 3c. In contrast (Fig. 6b), SPM levels are much lower during high river discharge (0.3 kg/m^3). A turbid area around 1.5 kg/m persists near the bottom along the first kilometres. Upstream the salt wedge (KP 10), the water column is both weakly turbid and brackish water. Along the salt wedge, a two-layer behaviour probably happens. Near the bottom, strong vertical variation in SPM is co-located with the salt wedge. SPM is decreasing from 1 to 0.1 kg/m^3 from the bottom to the mid depth. Until the water surface, a fresh water layer with SPM around 0.1 kg/m^3 is flowing above the saline layer.

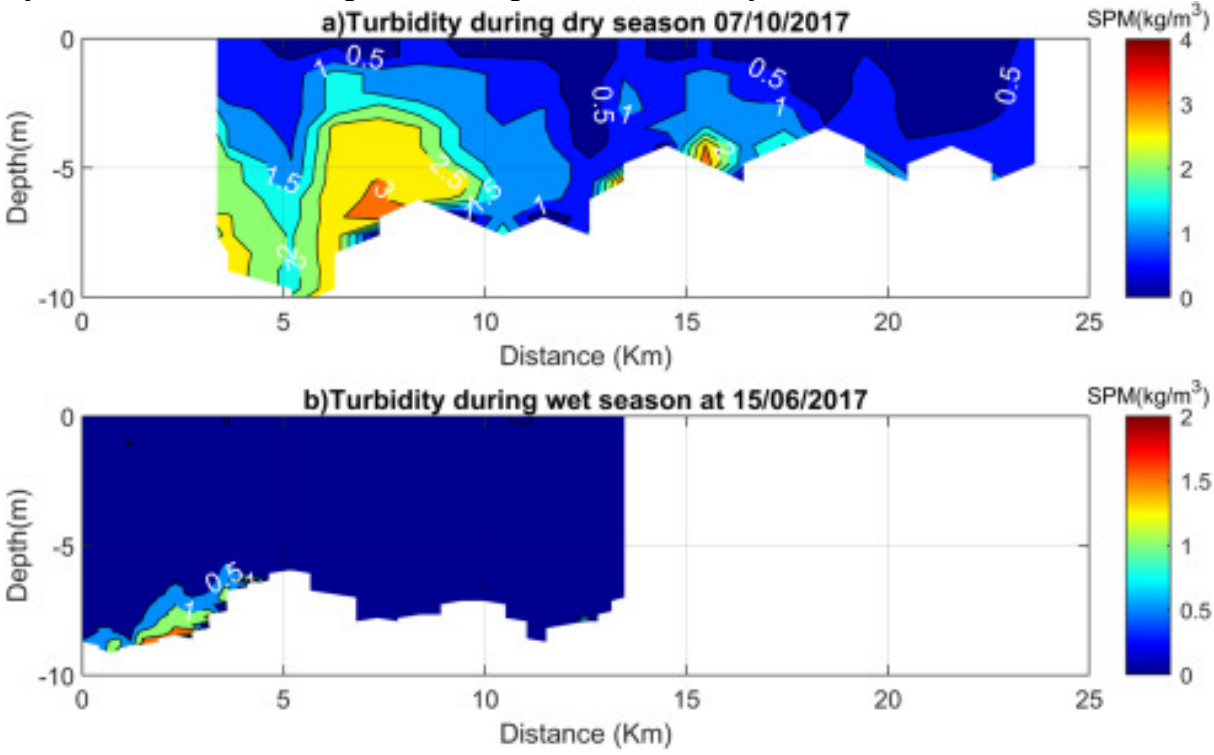

Fig. 6. Measured SPM levels measured along the navigation channel at high tide during dry and high river discharge.

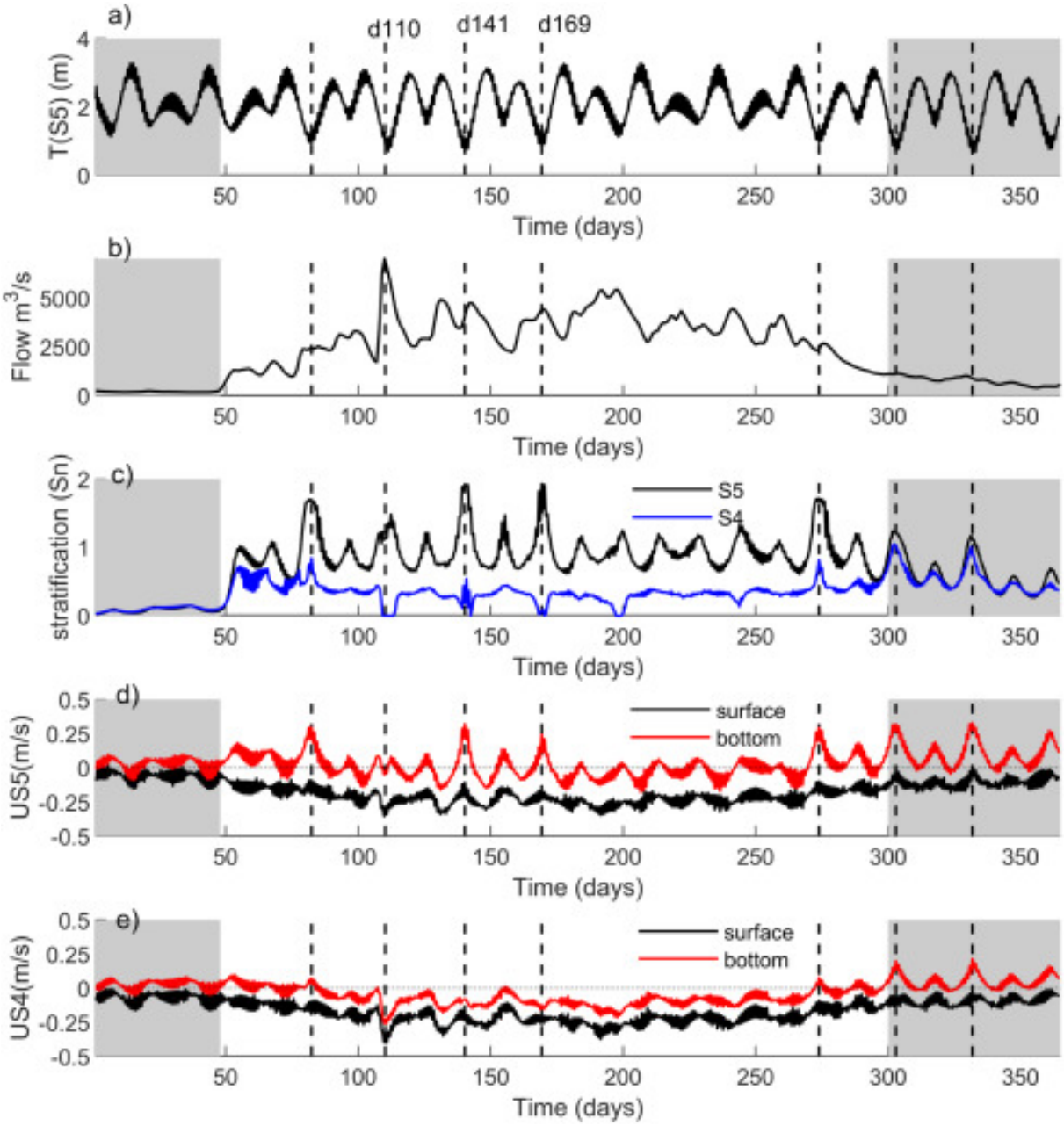

Fig. 7. Time series of tidal range, river discharge, stratification, residual currents at station S5 and S4.

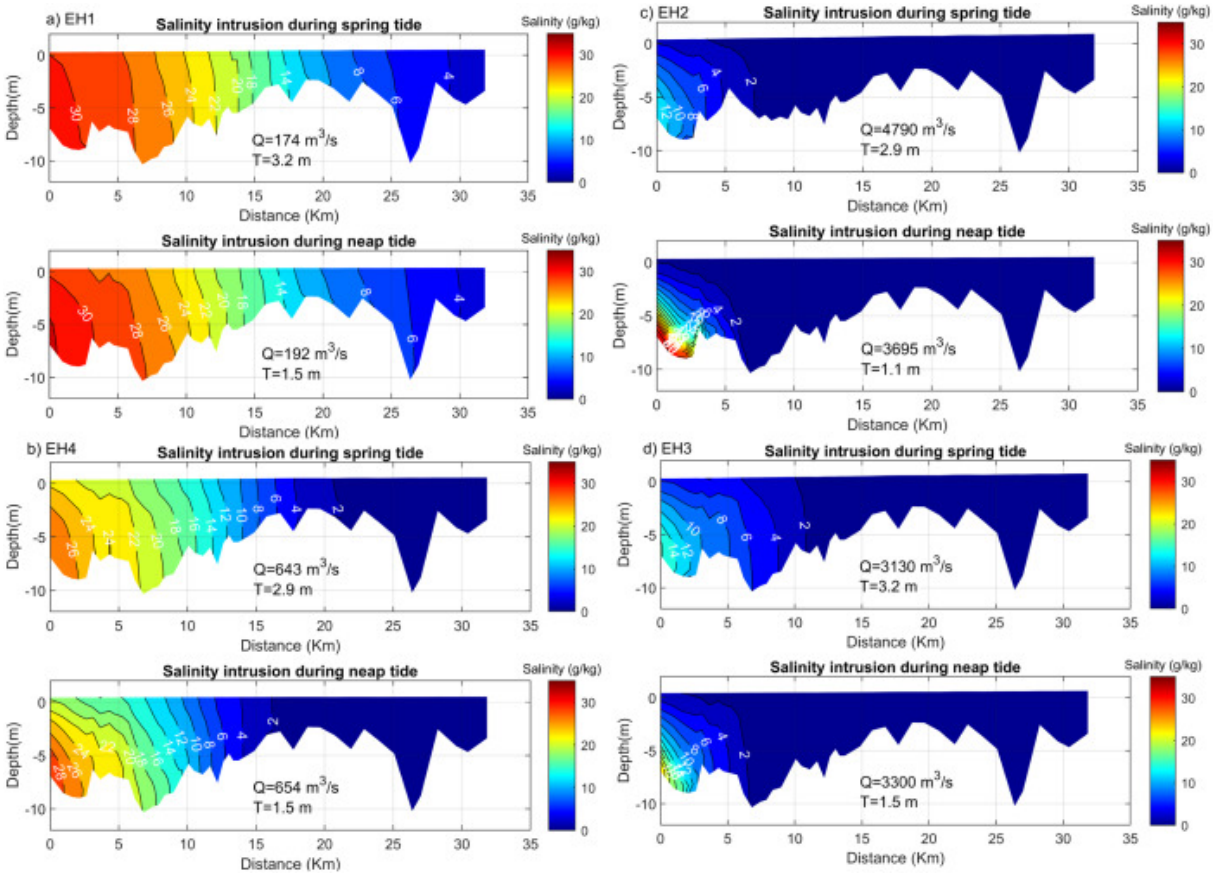

Fig. 8. Semi-diurnal tidally average salinity distribution along the longitudinal transect: (a) low river discharge EH1, (b) low river discharge EH4, (c) high river discharge EH2 and (d) high river discharge EH3. Q is the flowrate and T the tidal range.

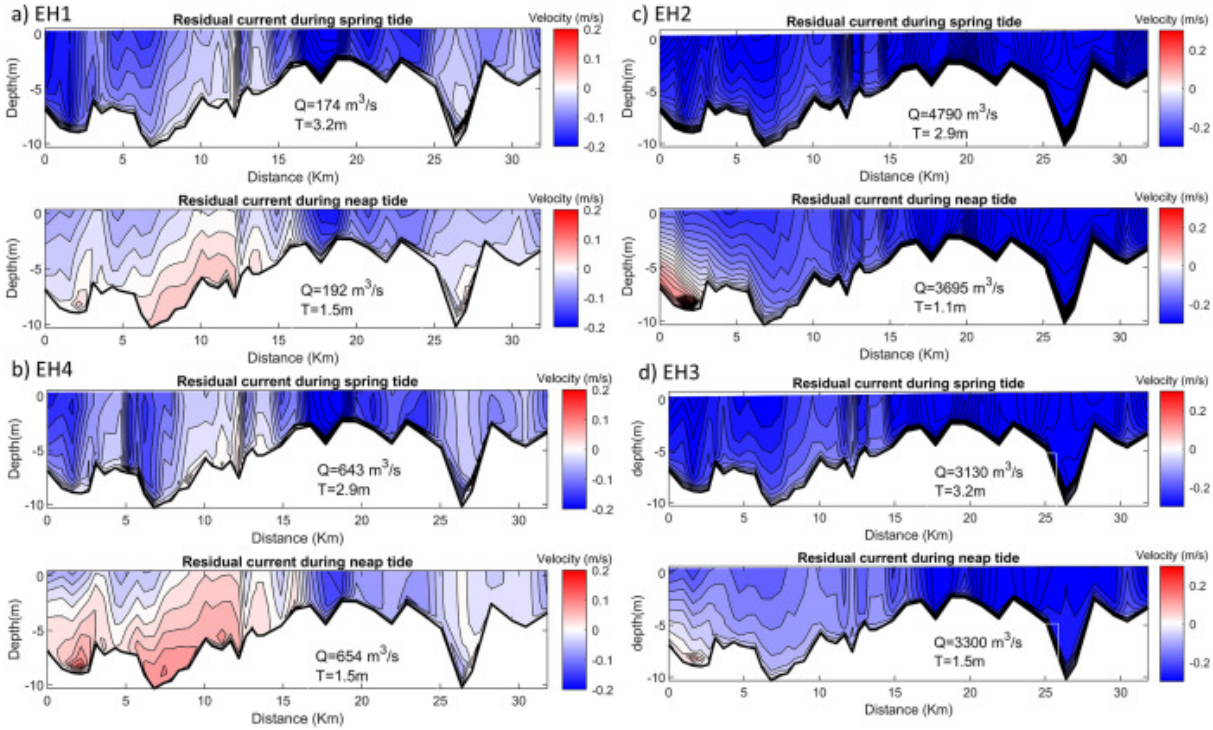

Fig. 9. Semi-diurnal residual current along the longitudinal transect during low river discharge (EH1(a), EH4 (b)) and during high river discharge (EH2(c), EH3 (d)).

5.4. Numerical analysis of salt intrusion under different river discharge and tidal range

One-year simulation is performed from November 2016 to October 2017 to explore the influence of discharge and tidal range on the saline intrusion and stratification patterns. A 40 days spin up simulation with a constant discharge (mean value of October 2016) was performed in order to initialize the hydrodynamic variables and salinity distribution. Then a one-year simulation with a time series of daily discharge is performed with initial conditions provided by the spin-up simulation. Time evolutions of realistic tidal range and discharge are illustrated on Fig. 7a and b (other subplots are discussed later). It starts with a pronounced dry period about 50 days, followed by a long high river discharge about 250 days and then it finishes with another dry period with moderate flow rates. Extracted events for the analysis match with the four shipboard surveys. For dry periods, saline intrusions are extracted for both discharge 200 m^3/s, 700 m^3/s. For each hydrological condition, no significant change in discharge value is observed along the considered neap and spring tidal cycle. For the high river discharge, analysed events are 4790 m^3/s and 3120 m^3/s for spring tide whereas lower values 3700 m^3/s and 3300 m^3/s are observed for neap tides. Fig. 8 represents the tidally averaged salinity distribution in a single along-channel section (transect 1 as in Fig. 1).

During river discharge lower than 200 m^3/s, well-mixed conditions are observed at both spring tide and neap tide (Fig. 8a). Salt water (S 30 g/kg) is only observed for such low discharge and along the 3 first kilometres. For the other discharge configurations, brackish water (S 30 g/kg) is observed inside the estuary. When the discharge rises up to 650 m^3/s, it generates more vertical variation until approximately km 12 (Fig. 8b). In this condition, brackish water penetrates less into the river than in the case of very low discharge (200 m^3/s). For instance, isohaline 4 propagated until 30 km in case of very low discharge whereas it only reaches between km 15 and km 17 in case of discharge up to 650 m^3/s.

In contrast, with high discharge conditions, brackish water is generally transported into the estuary during spring tides and it is expelled out of the estuary during neap tides (Fig. 8c, d). The brackish water convergence front remains confined near the mouth during the high discharge. Neap tides of the high discharge also feature significant stratification at the mouth. Stratification is less pronounced during spring tides than during neap tides. Increase of discharge tends to enhance stratified conditions as it can be clearly seen with two cases of neap tides. Indeed, the case with a discharge of 3695 m^3/s has higher salinity at the bottom than the case with a river discharge of 3300 m^3/s. The effect of wind on such a pattern would need to be further investigated even if less influence is expected during high flowrates.

5.5. Numerical analysis of the residual current and its variability

Tidally-averaged currents are computed in order to estimate the main residual flow direction and to identify the conditions favourable for inflow of salinity and therefore oceanic mud. A single longitudinal view along the navigation channel from the mouth until the upper station S2 is first extracted (Fig. 9) under different tidal ranges and river flows with both low and high discharges.

Fig. 9(a, b) shows a complex residual circulation pattern for the low river discharge. Inflow close to the bottom can be observed approximately from river mouth to km 15. Inflow is restricted near the bottom during spring and covers until mid-depth during neap. Flowrate about 700 m^3/s leads to stronger inflow than with a 200 m^3/s discharge. Surface residual current is still mainly seawards except between KP 7 to KP 13 (neap cases) where the residual currents are mainly oriented across the channel. From KP 15 to upstream, the residual current is totally ebb dominated except a local circulation noticed at the deepest part KP 22. This area displays islands with trenches and tributaries. For the last kilometres where the depths are shallower, the residual currents are seawards.

During the spring tide with discharge higher than 3000 m^3/s (Fig. 9c, d), the flow is entirely ebb-directed or fluvial dominated. Strong seaward surface flow associated with immobile bottom layer occurs at some locations along the channel. Residual velocity magnitudes in the shallow areas are much greater than in the deepest parts of the channel. During neap tide and high discharge, residual currents are still mainly seaward even if a circulation zone can be noticed at the mouth. A stronger landward flow is indeed present on the first kilometres from the mouth where stratification pattern is also noticed (Fig. 8c&d).

6. Discussion

From the results section, different insights related to the Maroni dynamics can be summarized. Under high river discharge conditions (3000 m^3/s), high turbidity levels are noticed near the bottom along a

few kilometres only in the lower estuary (Fig. 6). LWS durations are much longer than HWS (Fig. 2) and residual currents (Fig. 9c & d) are seaward in the whole water column, except at the most downstream area, where a two-layer flow has been noticed. Such high river discharge induces stronger ebb velocities and longer ebb than flood duration. Near the mouth, a local salt wedge close the bottom coincides with fluvial advection near the surface although in the central and upper reaches the fluvial advection dominates the whole water column. This feature is a particularly interesting observation as it supports the existence of two distinct sources of fine sediment. The first one corresponds to a highly concentrated (1 kg/m^3) area probably fed mainly by mud bank and shifting seasonally according to flowrate variation. The second one ranging below 0.15 kg/m is brought from upstream by river freshets. Under very low flowrate (200 m^3/s), the estuary is mostly well mixed, high values of salinity and SPM are observed until upstream S2 station. Up to now, this is the first time that such high values are reported at such an upstream location. Between 2014 and 2016, dry periods have lasted longer than usual and high discharge events have been shorter and weaker (Abascal-Zorrilla et al., 2020), which can explain unusual high turbidities. It is hypothesized that the presence of mud until Saint Laurent results mainly from a higher contribution of tidal pumping since HWS durations are much longer than LWS and also from a smaller contribution of bottom inflow. Under moderate low river discharge, EH4 (700–1000 m^3/s), the estuary can be turbid until KP 15 (Fig. 6). In such a configuration, the HWS durations are slightly higher than the LWS (Fig. 3). Mud presence is probably due to a combination of a small contribution of tidal pumping and a higher contribution of inflow near the bottom (Fig. 9b). These preliminary conclusions need to be further confirmed by a consistent analysis of sediment transport.

From our results, the mouth corresponds to the most active area in terms of sediment dynamics, stratification, residual current. Moreover, it corresponds to the main source of fine sediment and the zone of exchange between the mud bank and the upper reaches of the estuary. It is thus now proposed to first further analyse the seasonal variation of the stratification patterns in this area. Numerical analysis of the residual current also identifies that the inflow in the navigation channel propagates more upstream inside the central part during low river discharges. Therefore, particular attention is then paid, for flow configurations with low river discharge conditions, on: (1) the neap–spring variation at different lateral sections; and (2) the circulation patterns in the central estuary during neap tide. Finally, the obtained results are put in perspective in regards to other regional studies.

6.1. Seasonal variations in stratification patterns

Time series of stratification number Sn [−] and residual current U [m/s] are extracted at station S5 and station S4 from the one-year simulation. The seasonal variations in stratification patterns for both stations are plotted in Fig. 7c.

At station S5, salinity stratification (Sn) describes a well-marked seasonal and spring–neapvariation controlled by both tidal ranges and river discharges (Fig. 7a&b). Larger tidal ranges reckon more vertical mixing and less stratification. Stratification is more developed under smaller tidal range (neap tides), e.g. day 141 (T m), day 169 (T m) and high river discharge. In the case of extremely low river discharge (day 0 to day 48, river flow less than 400 m^3/s), the stratification number is very small (average of 0.15) suggesting that the estuary is well-mixed. However, in case of a moderately low river discharge (day 300 to day 350) with river flow between 400 and 1200 m^3/s, salinity stratification number stands within 0.3 and 1.2 with an average of 0.6. It suggests a partly stratified estuary. In this case, major changes in river discharge has contributed to increase the saline stratification. For river discharge larger than 2660 m^3/s (day 100 to day 300), stratification number ranges from 0.6 to 1.9 (with an average of 0.94) which corresponds to strong stratification or even salt wedge. The change in stratification number due to flowrate variation exhibits each of three states of stratification: well-mixed, partially mixed and highly stratified. The relationship between stratification number and tidal range and stream flow, was developed by Vijith and Shetye (2012) by an estuarine stratification diagram primary based on tidal range number and runoff number. This diagram has successfully been applied to explain stratification of monsoon Mandovi estuary, which varies from well-mixed to highly stratified. In the case of the Maroni estuary, under high river discharge conditions (river discharge larger than 2660 m^3/s), the stratification number at station S5 (Sn5_wet) was found to be in relationship with tidal range (T). This relation can be illustrated by Eq. (1) as follow: (1)with R and -value 0.05.

At station S4, located upstream the converging section and thus already under higher river influence than S5, stratification number Sn features variation from 0 to 1 and displays insignificant correlation

with the tidal range. Comparing the evolutions at S4 and S5, the stratification numbers are almost the same for low river discharge and they behave quite differently during high river discharge. At S4, high stratification is observed during discharge within 400–1200 m^3/s flow (day 300 to day 350). The period from day 300 to day 365 is a dry period but moderate and quite stable flow rates. Thus, salinity intrusion develops further upstream, so the behaviour of stratification at S4 and S5 is quite the same.

When the river flow is very high and coincides with the small tidal range, the whole salt wedge is expelled out of the estuary. Salinity is only observed at S5 which leads to Sn values near zero at S4. Consequently, a higher stratification value of S5 coincides with a minimum value of stratification of S4 (e.g. days 110 and 169, Fig. 7). For day 141, the stratification reaches a maximum value at S5. At S4, the behaviour is less clear since the stratification reaches a maximum and then after a minimum value probably due to significant flowrate variation during the previous days.

In contrast to the stratification number, residual current near the bottom at both station S4 and S5 are controlled by tidal range, stratification number and river discharge. It can be illustrated through a multiple regression comparing residual current near the bottom (US4_bottom, US5_bottom) against tidal range (T), stratification (Sn) and river flow (Q) as Eqs. ((2), and (3)). (2)with R and -value 0.05 (3)with R and -value 0.05.

Residual inflow (positive values) at station S4 mostly occurs when river flow is less than 2660 m^3/s and tidal range is less than 2.75 m. It strongly depends on tidal ranges as smaller tidal ranges (neap tides, T 1 m) develop stronger inflow near the bottom. The strongest inflow (0.2 m/s) occurs in case of low neap tide (T 0.64 m), stratification of 0.89 and river flow of 900 m^3/s. Contrarily, outflow mostly occurs during the high river discharge and it is mainly controlled by river discharges. Higher river discharge logically induces higher outflow current since the strongest outflow (−0.25 m/s) can be detected at peak discharge of 7000 m^3/s (day 110 in time series).

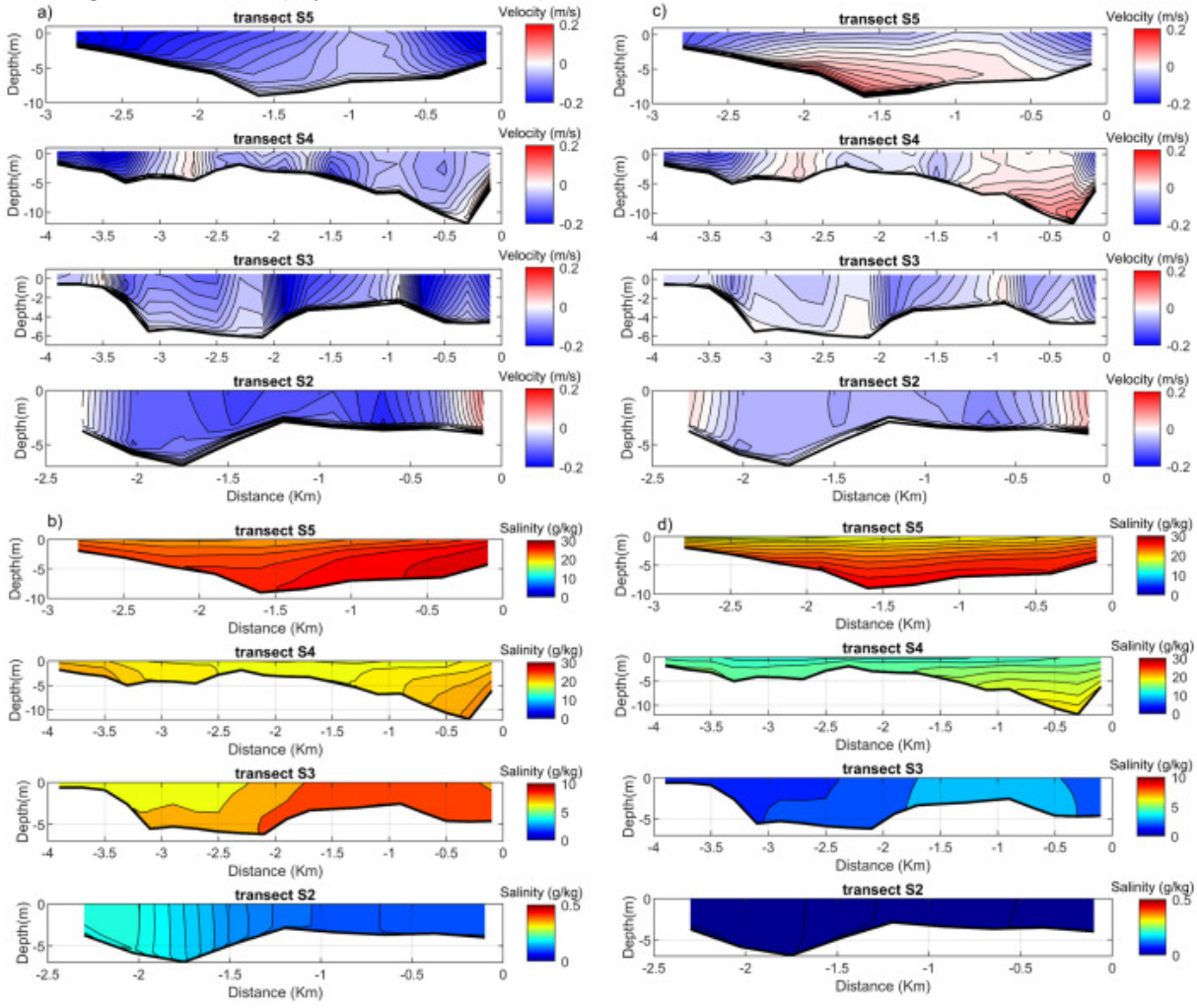

Fig. 10. Distribution of longitudinal residual current and residual salinity in cross section during the low river discharge EH4 (Positive values correspond to landward current and

negative values correspond seaward current); a, b depicts spring tide, c and d depict neap tide. Distance 0 km is located at the most east side of the river section (French Guiana side).

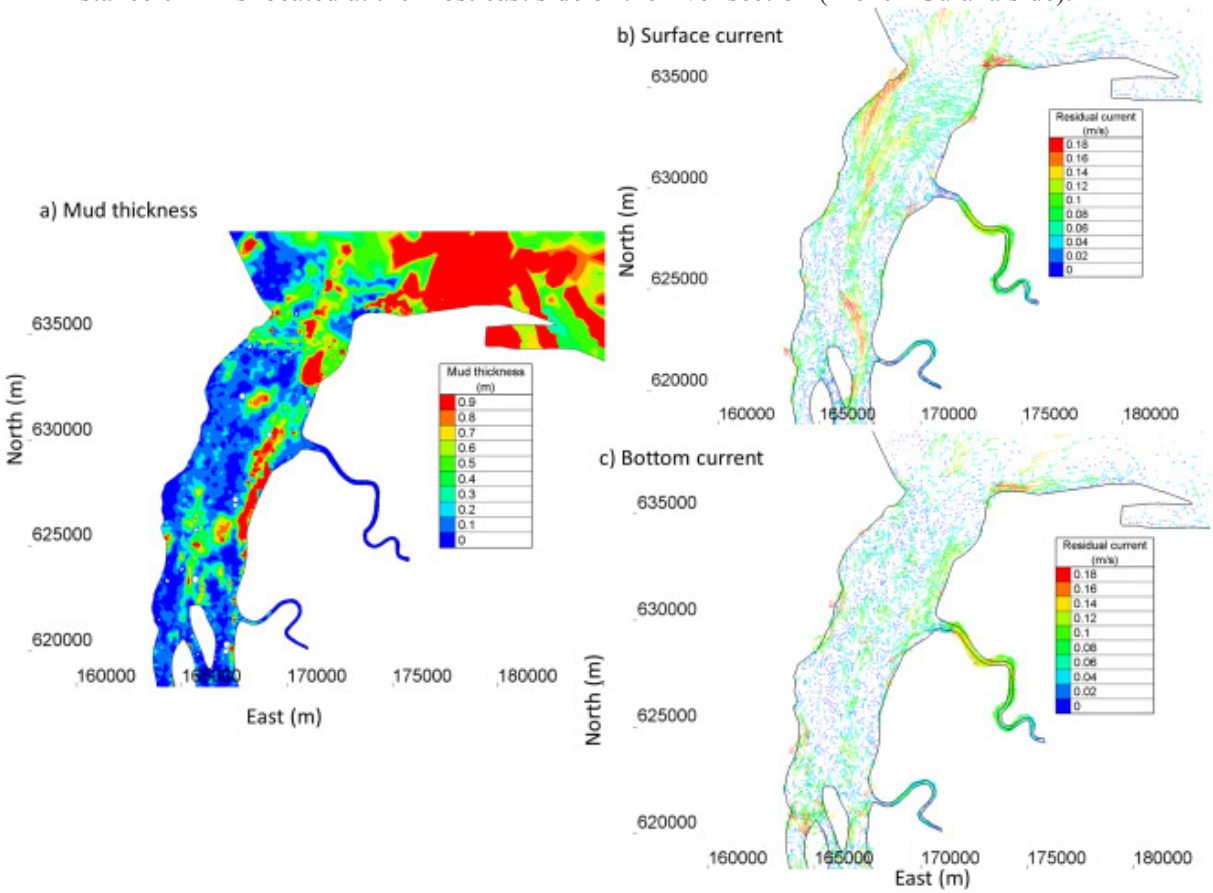

Fig. 11. Fluid mud deposit and horizontal residual current during neap tide with moderate low river discharge.

More downstream, the bottom residual current at station S5 is mainly directed upstream for a wide range of river discharge both during dry and high river discharge. It is however more marked during dry periods. When the river flow is larger than 2660 m^3/s, inflow only occurs during neap tides when the tidal range is lower than 2.3 m. Outflow is mostly observed during high river discharge period and sometimes during low river discharge periods. In case of very low flowrate (day 1 to day 48, river flow less than 400 m^3/s), outflow only occurs when the tidal range is greater than 2.2 m while for moderate flowrates within 400–1200 m^3/s (day 300 to day 350) outflow only occurs when the tidal range is larger 2.6 m. The strongest inflow at S5 (0.32 m/s) appears at the same time as the strongest inflow at station S4 (in case of low neap tide T 0.64 m, stratification of 0.89 and river flow of 900 m^3/s). In general, near-bottom residual currents at station S5 are mainly controlled by the tide than by the river flow, since inflow mostly occurs during neap tides and outflow mostly occurs during spring tides.

6.2. Processes driving the circulation during low river discharge

Up to now, the circulation has been analysed in a single along estuary transect. This transect is located in the navigation channel in the deeper area and it is not thus representative of the whole cross-section flow. To complete this analysis, lateral views at different cross sections are extracted to further examine the flow pattern and its lateral variation with a moderate low flowrate during the low river discharge for spring (Fig. 10a) and neap tides (Fig. 10c). During spring tide (Fig. 10a), outflow residual current is observed almost along the whole water column at all transects from S5 to S2 with maximum outflow current of 0.2 m/s found at some shallow areas of transect S5, S4 and S3. Outflow mainly happens in the deep channel whereas some inflow occurs over shoals. The barotropic tidal currents seem to mainly control residual current during spring tide. Distributions of residual salinity (Fig. 10b) indicates slight lateral variation from transect S5 to S3 and higher surface salinity compared to salinity level reached in

neap tide. Near bottom inflow is observed at the deepest part of the transect S4 where vertical variation in salinity is stronger than in other parts (Fig. 10b). Such inflow could be thus induced by the density-driven flow.

In contrast during neap tide (Fig. 10c), a two-layer of current can be clearly observed at transect S5, between KP-0.5 and KP-2, with strong inland flow at the bottom and slight outflow near the surface. Inflow currents are also observed in the deepest waters of transect S4 as in spring tides but it is more developed along the water depth and much stronger (from right bank side to KP 1.5) with residual current reaching 0.12 m/s near the bottom. At the left bank side of transect S4, a strong outflow current is observed near the surface (magnitude of −0.15 m/s). Residual circulation is also observed at transect S3 (KP 15) but with slight inflow near the bottom and stronger outflow near the surface. At station S2 (Fig. 10c) in both cases spring and neap tides, flow pattern is almost symmetric with outflow in the main channel while inflow appears at both lateral sides. Such symmetric pattern in exchange flow has also been noticed by Valle-Levinson (2008) using a semi analytical model with high frictional condition with moderately sloped cross-section. The evidence of the density-driven inflow is also clearly observed during the neap tides. Stronger inflows occurring at the deepest channel at S4 and S5 correspond to a strong vertical variation of salinity in this region. At transect S3 and S4, lateral circulation in velocity can be observed where inflow at some shallow parts occurs with presence of depth variations.

During spring tides, higher tidal range enhances mixing and thus leads to weaker vertical variation in salinity and a reduction of density-driven flow. For instance, at S5 from spring (day 323, T 3 m) to neap tide (day 331, T 0.63 m), Sn is increasing from 0.38 to 1.1. Therefore, weak inflow current is thus observed during spring tides. In contrast, tidally averaged salinity was more stratified during neap tide than during spring tide thus density-driven flow component is overwhelmed which results in a stronger residual circulation.

Increase of mixing during spring tides leads to reduced exchange flow as hypothesized by Geyer and Cannon (1982) and documented in several estuaries (Geyer et al., 2000, Bowen and Geyer, 2003, Weisberg and Zheng, 2003, MacCready and Geyer, 2010, Monismith and Fong, 1996, Stacey et al., 2010). Uncles and Stephens (2011) also mentioned an increase of surface salinity at high water because of enhanced vertical mixing in the Tavy estuary (UK) during spring tide.

Similarly, stronger stratified condition and associated salt net transport into the estuary has also been observed during neap tides in the Hudson estuary (Wang et al., 2015, Wang and Geyer, 2018) or in the Danshuei river in Taiwan (Chen and Liu, 2016). According to Wang et al. (2017), stratification may be regarded as the competition between tidal stirring and mean straining by the exchange flow. Tidal stirring transports salt up from the bottom to the surface, which decreases the stratification. When exchange flow is the greatest during neap tide, tidal stirring is weak. So, the influence of flow exchange exceeds tidal stirring and it thus continues to increase stratification. As tidal amplitude increases (spring tides), the influence of tidal stirring exceeds the exchange flow, so the stratification decreases.

Horizontal maps of surface and bottom residual currents are plotted (Fig. 11) to highlight the general circulation (along/across channel component) during neap tide combined with moderate low river discharge (700 m^3/s). The surface currents (Fig. 11b) are mainly seaward with stronger magnitude along the west channel (Suriname) whereas inflow currents near the bottom (Fig. 11c) are observed in the main channel at the right bank side (French Guiana). These results are in line with observations of Jolivet et al. (2019) and support the hypothesis of Ross et al. (2019). Analysis of bathymetric survey performed by Jolivet et al. (2019) supplemented by Gardel et al., this issue reveals a relatively straight single channel from the river mouth running north–northeast and a secondary less pronounced channel extending along the Suriname coast (Fig. 1). Based on analysis on ADCP surveys along and across the channel during high river discharge in 2018, Ross et al. (2019)proposed a simplified diagram of the circulation. They highlight the presence of an ebb channel on the west side and a flood channel on the east side. In our model results, outflow (ebb current) is almost present along the Suriname channel near the mouth. More upstream, the ebb channel crosses the estuary and reaches the east side near the island. Inflow (flood current) enters along the main channel on the east side. Interestingly, the plan views of residual currents at the bottom (Fig. 11c) could also be used to explain the distribution of measured mud thickness in the field. The fresh mud thickness was measured in October 2017 (Fig. 11a) corresponding to the same simulation period. Fresh mud deposits on the east side around the navigation channel occur in a zone characterized by low residual current and located just upstream inflow zone. Mud deposits near the inland seem rather come from across channel exchange from the flood channel to shallow areas.

6.3. In regard to the regional context

Despite many studies have focused on the coastal mud bank migration during the last decades, the dynamics of the several estuaries located along the Guiana shoreline are still poorly described. More particularly, few research efforts have focused on interactions between such estuaries and their muddy coastal environment (Orseau et al., 2017, Toorman et al., 2018).

Based mainly on analysis of geographic features, a classification of the estuaries along the Guiana coast has been drawn and four main types of estuaries have been identified (Gardel et al., 2019). The first type of estuaries has river mouths oriented perpendicularly to the coast, associated with relatively large-discharge rivers. A subtype of this first type is a transitional river-mouth morphology towards a delta. This is the case for the Maroni and Essequibo estuaries Gardel et al., this issue. The third type of estuaries has low flowrate and its morphodynamic features are thus strongly influenced by the mud bank, and river mouths are diverted westward (the direction of regional alongshore sediment transport) by prograded mud capes and spits. The fourth type of estuaries are fixed by headlands of Precambrian basement rocks.

About ten estuaries are spread along the coast of French Guiana. Up to now, more attention has been paid on hydro-sedimentary dynamics of the Mahury (type 4, Orseau et al., 2017) and Maroni (type 2) estuaries as they host activities. This exploratory study allow to expand the proposed classification with the introduction of physical consideration. In fact, most of the other estuaries belong to type 3 with low flowrate and strong morphodynamic impact of the mud bank. Except Sinnamary estuary and its dam for electricity production, they are less practical reasons to fund their studies and they are thus even less documented. Additional research efforts are thus still needed to provide a recent and complete physical analysis of the Guiana estuaries.

Actually, the Maroni estuary is the unique type 2 in French Guiana. Other similar estuaries are Corentyne River between Suriname and Guyana and Essequibo River in Guyana. As the Maroni, these two estuaries are subjected to heavy metal contamination due to gold mining activities (Howard et al., 2011). More knowledge in circulation may help to better predict the sediment fluxes and remobilization of polluted particles. Between 2014 and 2018, a mud bank has crossed the Mahury estuary (Orseau et al., 2020). Orseau et al. (2017) have performed in situ monitoring of the Mahury estuary between 2013 and 2016. Their analysis based on residual transport pointed out inflow of sediment fluxes during the low river discharge and still some inflow during high river discharge at the mouth for spring tide. According to Orseau et al. (2020), the mud bank near the Mahury estuary took almost 4 years to migrate across the mouth and only one bank has by-passed the estuary during the 10 years of observation.

Similarly, to the Mahury configuration, another mud bank has approached the mouth of the Maroni estuary since 2015 (Jolivet et al., 2019). Results from the Mahury estuary cannot be fully transposed because both estuaries are quite different in terms of fluvial discharge and geometry features. Because of the strength of Maroni discharge (Anthony et al., 2013), the mud bank is deviated offshore and it takes more time to cross the mouth. It thus creates a more continuous presence of mud banks at the mouth compared to the other smaller estuaries. According to our results, sediment inflow will occur mainly when the mud bank is near the flood channel on the French Guiana side. When the mud bank migrates through the mouth, it is pushed away by the river and then it by-pass the ebb channel on the Suriname side. Less mud inflow is thus expected. This assumption needs to be further investigated since offshore the mud-wave interaction becomes more significant and more research efforts are thus needed to analyse this effect on flow circulation.

Even if the Maroni displays sandier bed sediment than the other Guiana estuaries, muddy materials and higher salinity level have been observed up to Saint Laurent during a well pronounced low river discharge in 2016. During drier year that would probably happen more often in a near future due to climate change, this estuary can be as affected as the other estuaries by a mud bank presence. Similarly, as on the Mahury, the river flowrate also appears as a key parameter controlling the dynamics (Orseau et al., 2020).

7. Conclusions and perspectives

Field surveys have been conducted under low and high river discharge season for different tidal conditions. To enlarge the analysis, a 3D hydrodynamic model has been used to determine stratification patterns and associated residual currents under a wide range conditions.

Tidal data reckon an increase of the tidal amplitude in the downstream part of the estuary due to convergence. Further upstream friction effect dominates and the tidal range decreases. From in-situ measurements, a well contrasted behaviour has been observed between the low and high river discharge periods. During the high river discharge period, the river dominates estuarine dynamics, with stronger ebb currents at all measurement stations. Salinity is only observed near the mouth during high tide and the estuary is nearly fresh during low tide. The along channel in situ survey has pointed out a turbidity maximum which seems to persist at the bottom near the mouth during high river discharge. Near the surface, an upper layer with lower SPM and salinity levels is observed. During the low river discharge period, the estuary appears highly turbid until the central reaches.

The model results identify a well-mixed estuary during very low river discharge (river discharge lower than 400 m^3/s), and it turns into partially stratified estuary under moderately low river discharge (river discharge ranging between 400 m^3/s and 1200 m^3/s) and it becomes strongly stratified or salt wedge during the high river discharge period (river discharge is greater than 2600 m^3/s). Residual inflow near the bottom along navigation channel mostly occurs during the low river discharge period when the estuary is between well-mixed or partly stratified. Stronger inflow currents are more developed during neap tides with moderately low river discharge due to an increase of density-driven flow. In fact, the strongest inflow current is developed in case of low neap tide with a river discharge of 800–900 m^3/s. Under such flowrate conditions in neap tide, residual currents are landward from the bottom to mid depth until the first KP15 from the mouth. The extension of the inflow area matches with the zones where high concentration level and mud deposit have been observed. Inflow channel starts from the location of the mud bank near the mouth and extends along the navigation channel in the eastern part. This most favourable flow pattern for mud income however requires that sediments are available and erodible for such flow conditions.
Developments on the model are ongoing to include sediment transport and the wave influence. Once, it would be interesting to analyse how these numerical results evolve once the sediment dynamics and associated stratification effect are added inside the model. Further efforts are still needed to analyse the influence of the tributaries and the mangrove on the circulation and to characterize the estuarine dynamic upstream Saint Laurent.

CRediT authorship contribution statement

Anh T.K. Do: Performing model simulation, Data analysis, Graphical visualisation, Drafting the manuscript. **Aldo Sottolichio:** Conceptualization and design of the study, Data interpretation, Manuscript critical review and editing. **Nicolas Huybrechts:** Performing model simulation, Data analysis, Graphical visualisation, Drafting the manuscript. **Antoine Gardel:** Conceptualization and design of the study, Data interpretation, Manuscript critical review and editing.

Declaration of Competing Interest

The authors declare that they have no known competing financial interests or personal relationships that could have appeared to influence the work reported in this paper.

Acknowledgements

The authors would like to thank the “Service d’Hydrographie Océanique Maritime (SHOM)” for providing bathymetric data on the continental shelf, the Direction de l’Equipement de l’aménagement et du logement de la Guyane (DEAL)” for the bathymetric data inland, tidal data and their financial support. We are also grateful to Sylvain Morvan, Tanguy Maury, Sandric Lesourd and Guillaume Detandt who helped with data collection. Funding was also provided by the European Fund for Regional Development (ERDF) programme OYAMAR and by the French Guiana Office of Water under the EFHEMAR project to support the in situ work. Anh, T.K. Do, post doc position has been funded by the Inthrig project from ANR Carnot Cerema Effiscience.

References

Abascal-Zorrilla, N., Vantrepotte, V., Huybrechts, N., Ngoc, D.D., Anthony, E.J., Gardel, A., 2020. Dynamics of the estuarine turbidity maximum zone from landsat-8 data: The case of the Maroni River Estuary, French Guiana. Remote Sens. 12 (13), 2173. http://dx.doi.org/10.3390/rs12132173.

Allison, M.A., Lee, M.T., Ogston, A.S., Aller, R.C., 2000. Origin of Amazon mudbanks along the northeastern coast of South America. Marine Geology, 163(1-4), 241-256. https://doi.org/10.1016/S0025-3227(99)00120-6.

Anthony, E.J., 2004. Sediment dynamics and morphological stability of estuarine mangrove swamps in Sherbro Bay, West Africa. Marine Geology, 208(2-4), 207-224. https://doi.org/10.1016/j.margeo.2004.04.009.

Anthony, E.J., 2006. The muddy tropical coast of West Africa from Sierra Leone to Guinea-Bissau: geological heritage, geomorphology and sediment dynamics. Africa Geoscience Review, 13, 227-237.

Anthony, E.J., Dolique, F., 2004. The influence of Amazon-derived mud banks on the morphology of sandy headland-bound beaches in Cayenne, French Guiana: a short-to long-term perspective. Marine Geology, 208(2-4), 249-264. https://doi.org/10.1016/j.margeo.2004.04.011.

Anthony, E.J., Gardel, A., Gratiot, N., Proisy, C., Allison, M.A., Dolique, F., Fromard, F., 2010. The Amazon-influenced muddy coast of South America: A review of mud-bank–shoreline interactions. Earth-Science Reviews, 103(3-4), 99-121. https://doi.org/10.1016/j.earscirev.2010.09.008.

Anthony, E.J., Gardel, A., Proisy, C., Fromard, F., Gensac, E., Peron, C., et al., 2013. The role of fluvial sediment supply and river-mouth hydrology in the dynamics of the muddy, Amazon-dominated Amapá–Guianas coast, South America: a three-point research agenda. J. South Am. Earth Sci. 44, 18–24. http://dx.doi.org/10.1016/j.jsames.2012.06.005.

Asp, N.E., Gomes, V.J.C., Schettini, C.A.F., Souza-Filho, P.W.M., Siegle, E., Ogston, A.S., ... Pereira, L.C.C., 2018. Sediment dynamics of a tropical tide-dominated estuary: Turbidity maximum, mangroves and the role of the Amazon River sediment load. Estuarine, Coastal and Shelf Science, 214, 10-24. https://doi.org/10.1016/j.ecss.2018.09.004.

Berthois, L., Hoorelbeck, J., 1968. Etude dynamique de la sédimentation dans trois cours d'eau de la Guyane française: la rivière Mahury, la rivière de Cayenne, et le fleuve Maroni.

Bomer, E.J., Wilson, C.A., Hale, R.P., Hossain, A. N. M., Rahman, F.A., 2020. Surface elevation and sedimentation dynamics in the Ganges-Brahmaputra tidal delta plain, Bangladesh: Evidence for mangrove adaptation to human-induced tidal amplification. Catena, 187, 104312. https://doi.org/10.1016/j.catena.2019.104312.

Bourret, A., Devenon, J.L., Chevalier, C., 2008. Tidal influence on the hydrodynamics of the French Guiana continental shelf. Continental Shelf Research, 28(7), 951-961. https://doi.org/10.1016/j.csr.2008.01.008.

Bowen, M.M., Geyer, W.R., 2003. Salt transport and the time-dependent salt balance of a partially stratified estuary. J. Geophys. Res.: Oceans 108 (C5), http://dx.doi.org/10.1029/2001JC001231.

Capo, S., Sottolichio, A., Brenon, I., Castaing, P., Ferry, L., 2006. Morphology, hydrography and sediment dynamics in a mangrove estuary: the Konkoure Estuary, Guinea. Marine Geology, 230(3-4), 199-215. https://doi.org/10.1016/j.margeo.2006.05.003.

Chapman, V. J., 1974. Salt marshes and salt deserts of the world. Ecology of halophytes, 3-19.

Chen, W.B., Liu, W.C., 2016. Modeling investigation of asymmetric tidal mixing and residual circulation in a partially stratified estuary. Environ. Fluid Mech. 16 (1), 167–191. http://dx.doi.org/10.1007/s10652-015-9421-4.

Chevalier, C., Baklouti, M., Ramamonjiarisoa, A., 2004. Modeling the influence of wind and rivers on current, salinity and temperature over the French Guiana continental shelf during the rainy season. Journal of Coastal Research, 1183-1197. https://doi.org/10.2112/03-0059R.1

Chevalier, C., Froidefond, J.M., Devenon, J. L., 2008. Numerical analysis of the combined action of littoral current, tide and waves on the suspended mud transport and on turbid plumes around French Guiana mudbanks. Continental Shelf Research, 28(4-5), 545-560. https://doi.org/10.1016/j.csr.2007.09.011.

Do, A.T.K., Huybrechts, N., Sottolichio, A., Gardel, A., 2019. Modeling and Quantification of Patterns of Salinity, Mixing and Subtidal Flow in the Maroni Estuary. In International Conference on Asian and Pacific Coasts (pp. 657-664). Springer, Singapore. https://doi.org/10.1007/978-981-15-0291-0_90.

Fettweis, M., Sas, M., Monbaliu, J., 1998. Seasonal, neap-spring and tidal variation of cohesive sediment concentration in the Scheldt Estuary, Belgium. Estuarine, Coastal and Shelf Science, 47(1), 21-36. https://doi.org/10.1006/ecss.1998.0338.

Froidefond, J. M., Pujos, M., Andre, X., 1988. Migration of mud banks and changing coastline in French Guiana. Marine Geology, 84(1-2), 19-30. https://doi.org/10.1016/0025-3227(88)90122-3.

Gardel, A., Gratiot, N., 2005. A satellite image–based method for estimating rates of Mud Bank Migration, French Guiana, South America. Journal of Coastal Research, 720-728. https://doi.org/10.2112/03-0100.1.

Gardel, A., Anthony, E., Huybrechts, N., Lesourd, S., Santos, V., Sottolichio, A., 2019. River estuaries of the Amazon-influenced Guianas coast: diversity and preliminary classification. In Geophysical Research Abstracts (Vol. 21).

Gardel, A., Anthony, E.J., dos Santos, V., Huybrechts, N., Lesourd, S., Sottolichio, A., Jolivet, M., Maury, T. (202x) Sediment dynamics and coastal progradation in the vicinity of the Maroni River mouth: control factors and transition from estuary to delta. Submitted to Regional Studies in Marine Science.

Geyer, W.R., Cannon, G.A., 1982. Sill processes related to deep water renewal in a fjord. Journal of Geophysical Research: Oceans, 87(C10), 7985-7996. https://doi.org/10.1029/JC087iC10p07985.

Geyer, W.R., Trowbridge, J.H., Bowen, M.M., 2000. The dynamics of a partially mixed estuary. Journal of Physical Oceanography, 30(8), 2035-2048. https://doi.org/10.1175/1520-0485(2000)030<2035:TDOAPM>2.0.CO;2

Gratiot, N., Gardel, A., Anthony, E.J., 2007. Trade-wind waves and mud dynamics on the French Guiana coast, South America: input from ERA-40 wave data and field investigations. Marine Geology, 236(1-2), 15-26. https://doi.org/10.1016/j.margeo.2006.09.013.

Hansen, D.V., Rattray Jr, M., 1966. New dimensions in estuary classification 1. Limnology and Oceanography, 11(3), 319-326. https://doi.org/10.4319/lo.1966.11.3.0319.

Hervouet, J.M., 2007. Hydrodynamics of free surface flows: modelling with the finite element method (Vol. 360). New York: Wiley.

Howard, J., Trotz, M.A., Thomas, K., Omisca, E., Chiu, H. T., Halfhide, T., ... Stuart, A.L., 2011. Total mercury loadings in sediment from gold mining and conservation areas in Guyana. Environmental monitoring and assessment, 179(1-4), 555-573. https://doi.org/10.1007/s10661-010-1762-3.

Jolivet, M., Anthony, E., Gardel, A., Brunier, G., 2019. Multi-decadal to short-term beach and shoreline mobility in a complex river-mouth environment affected by mud from the Amazon. Front. Earth Sci. 7:187. https://doi.org/10.3389/feart.2019.00187.

Jouanneau, J. M., Pujos, M., 1987. Suspended matter and bottom deposits in the Mahury estuarine system (French Guiana): environmental consequences. Netherlands journal of sea research, 21(3), 191-202. https://doi.org/10.1016/0077-7579(87)90012-3

Jounneau, J.M., Pujos, M., 1988. Suspended matter and bottom deposits in the Maroni estuarine system (French Guiana). Netherlands Journal of Sea Research, 22(2), 99-108. https://doi.org/10.1016/0077-7579(88)90014-2.

Kitheka, J.U., 1997. Coastal tidally-driven circulation and the role of water exchange in the linkage between tropical coastal ecosystems. Estuarine, Coastal and Shelf Science, 45(2), 177-187. https://doi.org/10.1006/ecss.1996.0189.

Lehfeldt R., Bloss S., 1988. Algebraic Turbulence Model for Stratified Tidal Flows. In: Dronkers J., van Leussen W. (eds) Physical Processes in Estuaries. Springer, Berlin, Heidelberg

Lugo, A.E., Snedaker, S.C., 1974. The ecology of mangroves. Annual review of ecology and systematics, 5(1), 39-64.

MacCready, P., Geyer, W.R., 2010. Advances in estuarine physics. Annu. Rev. Mar. Sci. 2 (1), 35–58. http://dx.doi.org/10.1146/annurev- marine- 120308- 081015.

Monismith, S.G., Fong, D.A., 1996. A simple model of mixing in stratified tidal flows. Journal of Geophysical Research: Oceans, 101(C12), 28583-28595. https://doi.org/10.1029/96JC02267.

Orseau, S., Lesourd, S., Huybrechts, N., Gardel, A., 2017. Hydro-sedimentary processes of a shallow tropical estuary under Amazon influence. The Mahury Estuary, French Guiana. Estuarine, Coastal and Shelf Science, 189, 252-266. https://doi.org/10.1016/j.ecss.2017.01.011.

Orseau, S., Zorrilla, N.A., Huybrechts, N., Lesourd, S., Gardel, A., 2020. Decadal-scale morphological evolution of a muddy open coast. Marine Geology, 420, 106048. https://doi.org/10.1016/j.margeo.2019.106048.

Pawlowicz, R., Beardsley, B., Lentz, S., 2002. Classical tidal harmonic analysis including error estimates in MATLAB using T_TIDE. Computers & Geosciences, 28(8), 929-937. https://doi.org/10.1016/S0098-3004(02)00013-4.

Ross, L., Sottolichio, A., Maury, T., Lesourd, S., Gardel, A., 2019. Intratidal and Subtidal Circulation in a Tropical Estuary during Wet Season: The Maroni, French Guiana. Journal of Marine Science and Engineering, 7(12), 433. https://doi.org/10.3390/jmse7120433.

Savenije, H.H., 1989. Salt intrusion model for high-water slack, low-water slack, and mean tide on spread sheet. Journal of Hydrology, 107(1-4), 9-18. https://doi.org/10.1016/0022-1694(89)90046-2.

Shimozono, T., Tajima, Y., Akamatsu, S., Matsuba, Y., Kawasaki, A., 2019. Large-scale Channel Migration in the sittang River estuary. Scientific reports, 9(1), 1-9. https://doi.org/10.1038/s41598-019-46300-x.

Sottolichio, A., Gardel, A., Huybrechts, N., Maury, T., Morvan, S., Lesourd, S., 2018. Premières observations de la dynamique hydro-sédimentaire de l'estuaire du Maroni (Guyane). In: Proceedings of the XV National Conference on Coastal and Civil Engineering (GCGC). La Rochelle, France. pp. 29–31.

Stacey, M.T., Brennan, M.L., Burau, J.R., Monismith, S.G., 2010. The tidally aver- aged momentum balance in a partially and periodically stratified estuary. J. Phys. Oceanogr. 40 (11), 2418–2434. http://dx.doi.org/10.1175/2010JPO4389. 1.

Toorman, E.A., Anthony, E., Augustinus, P. G., Gardel, A., Gratiot, N., Homenauth, O., ... Naipal, S., 2018. Interaction of Mangroves, Coastal Hydrodynamics, and Morphodynamics Along the Coastal Fringes of the Guianas. In Threats to Mangrove Forests (pp. 429-473). Springer, Cham. https://doi.org/10.1007/978-3-319-73016-5

Uncles, R. J., Elliott, R.C.A., Weston, S.A., 1985. Observed fluxes of water, salt and suspended sediment in a partly mixed estuary. Estuarine, Coastal and Shelf Science, 20(2), 147-167. https://doi.org/10.1016/0272-7714(85)90035-6.

Uncles, R.J., Stephens, J.A., 2011. The effects of wind, runoff and tides on salinity in a strongly tidal sub-estuary. Estuaries and coasts, 34(4), 758-774. https://doi.org/10.1007/s12237-010-9365-3.

Valle-Levinson, A., 2008. Density-driven exchange flow in terms of the Kelvin and Ekman numbers. J. Geophys. Res.: Oceans 113 (C4), http://dx.doi.org/10. 1029/2007JC004144.

Van Santen, P., Augustinus, P.G.E.F., Janssen-Stelder, B.M., Quartel, S., Tri, N.H., 2007. Sedimentation in an estuarine mangrove system. Journal of Asian Earth Sciences, 29(4), 566-575. https://doi.org/10.1016/j.jseaes.2006.05.011

Victor, S., Golbuu, Y., Wolanski, E., Richmond, R.H., 2004. Fine sediment trapping in two mangrove-fringed estuaries exposed to contrasting land-use intensity, Palau, Micronesia. Wetlands Ecology and Management, 12(4), 277-283. https://doi.org/10.1007/s11273-005-8319-1

Vijith, V., Shetye, S.R., 2012. A stratification prediction diagram from character- istics of geometry, tides and runoff for estuaries with a prominent channel. Estuar. Coast. Shelf Sci. 98, 101–107. http://dx.doi.org/10.1016/j.ecss.2011.12. 006.

Wang, T., Geyer, W.R., 2018. The balance of salinity variance in a partially stratified estuary: Implications for exchange flow, mixing, and stratification. J. Phys. Oceanogr. 48 (12), 2887–2899. http://dx.doi.org/10.1175/JPO-D-18- 0032.1.

Wang, T., Geyer, W.R., Engel, P., Jiang, W., Feng, S., 2015. Mechanisms of tidal oscillatory salt transport in a partially stratified estuary. J. Phys. Oceanogr. 45 (11), 2773–2789. http://dx.doi.org/10.1175/JPO-D-15-0031.1.

Wang, T., Geyer, W.R., MacCready, P., 2017. Total exchange flow, entrainment, and diffusive salt flux in estuaries. J. Phys. Oceanogr. 47 (5), 1205–1220. http://dx.doi.org/10.1175/JPO- D- 16- 0258.1.

Weisberg, R.H., Zheng, L., 2003. How estuaries work: A Charlotte Har- bor example. J. Mar. Res. 61 (5), 635–657. http://dx.doi.org/10.1357/ 002224003771815981.

Wells, J.T., Coleman, J.M., 1981. Physical processes and fine-grained sediment dynamics, coast of Surinam, South America. Journal of Sedimentary Research, 51(4), 1053-1068. https://doi.org/10.1306/212F7E1E-2B24-11D7-8648000102C1865D.

Willemsen, P.W.J.M., Horstman, E.M., Borsje, B.W., Friess, D.A., Dohmen- Janssen, C.M., 2016. Sensitivity of the sediment trapping capacity of an estuarine mangrove forest. Geomorphology 273, 189–201. http://dx.doi.org/ 10.1016/j.geomorph.2016.07.038.

Willmott, C.J., 1981. On the validation of models. Physical geography, 2(2), 184-194. https://doi.org/10.1080/02723646.1981.10642213.

Wong, Y. S., Tam, N. F., 2012. Asia-Pacific Symposium on Mangrove Ecosystems: Proceedings of the International Conference held at The Hong Kong University of Science & Technology, September 1–3, 1993 (Vol. 106). Springer Science & Business Media.

Wright, L.D., 1989. Dispersal and deposition of river sediments in coastal seas: models from Asia and the tropics. Netherlands Journal of Sea Research, 23(4), 493-500. https://doi.org/10.1016/0077-7579(89)90032-X.

Xiao, Y., Wu, Z., Cai, H., Tang, H., 2018. Suspended sediment dynamics in a well-mixed estuary: The role of high suspended sediment concentration (SSC) from the adjacent sea area. Estuarine, Coastal and Shelf Science, 209, 191-204. https://doi.org/10.1016/j.ecss.2018.05.018.